Silver nanoparticle-doped zirconia capillaries for enhanced bacterial filtration

Julia Wehling[a], Jan Köser[b], Patrick Lindner[c], Christian Lüder[c], Sascha Beutel[c], Stephen Kroll[a]* and Kurosch Rezwan[a]

*Corresponding author: *mail: stephen.kroll@uni-bremen.de, Tel. +49 (0)421 218 – 64933, Fax. +49 (0)421 218 – 64932*

[a] Advanced Ceramics, University of Bremen, Am Biologischen Garten 2, 28359 Bremen, Germany

[b] Department Sustainable Chemistry, Center for Environmental Research and Sustainable Technology, University of Bremen, Leobener Str. UFT, 28359 Bremen, Germany

[c] Institute for Technical Chemistry, Leibniz University of Hanover, Callinstr. 5, 30167 Hanover, Germany

ABSTRACT

Membrane clogging and biofilm formation are the most serious problems during water filtration. Silver nanoparticle (Ag_{nano}) coatings on filtration membranes can prevent bacterial adhesion and the initiation of biofilm formation. In this study, Ag_{nano} are immobilized via direct reduction on porous zirconia capillary membranes to generate a nanocomposite material combining the advantages of ceramics being chemical, thermal and mechanical stable with nanosilver, an efficient broadband bactericide for water decontamination. The filtration of bacterial suspensions of the fecal contaminant *E. coli* reveals highly efficient bacterial retention capacities of the capillaries of 8 log reduction values, fulfilling the requirements on safe drinking water according to the U.S. Environmental Protection Agency. Maximum bacterial loading capacities of the capillary membranes are determined to be $3x10^9$ bacterial cells/750 mm^2 capillary surface until back flushing is recommendable. The immobilized Ag_{nano} remain accessible and exhibit strong bactericidal properties by killing retained bacteria up to maximum bacterial loads of $6x10^8$ bacterial cells/750 mm^2 capillary surface and the regenerated membranes regain filtration efficiencies of 95-100 %. Silver release is moderate as only 0.8 % of the initial silver loading is leached during a three-day filtration experiment leading to average silver contaminant levels of 100 µg/L.

Keywords

Ceramic capillary membrane; macroporous; immobilized silver nanoparticles; bactericide membrane surface; silver leaching.

1. INTRODUCTION

Water purification technologies play an important role in reducing the risk of the dissemination of waterborne diseases or epidemic outbreaks that are caused by pathogenic microorganisms and viruses. Bacteria such as pathogenic serovars of *Salmonella* and *Vibrio cholerae* are responsible for severe diseases such as typhoid fever and cholera, and *E. coli* serves as an important indicator organism for fecal contaminations. Today, more than 250 serotypes of *E. coli* are known ranging from harmless gut commensals to severe pathogens [1], such as the virulent enterotoxigenic (ETEC), enteropathogenic (EPEC), and enterohaemorrhagic (EHEC) *E. coli*. Furthermore, viral infections can be spread via drinking water contaminations and highly infectious diseases are for example hepatitis A, poliomyelitis caused by the poliovirus or the severe acute respiratory syndrome (SARS) which is caused by the coronavirus.

Because bacterial contaminations in drinking water are nowadays the main reason for most of the upcoming diseases [2], the removal and inactivation of pathogenic coliforms and other microorganisms is therefore a field of great interest for both, industries and local authorities. These institutions are obliged to fulfill the requirements on water containing 0 fecal and total coliform counts in 100 mL of water intended for drinking [3]. Hence, small-sized water filtration systems that can be easily transported and provide sufficient amounts of purified water are of global interest [4].

Different filtration materials have been described for the use in water purification, such as polymeric materials like cellulose acetate (CA) [5], polysulfone (PS) [6], polyacrylonitrile (PAN) [7] or polyvinylidene fluoride (PVDF) [8], while polyethersulfone (PES) is the most commonly used material for membrane applications [9]. In contrast to polymeric filter materials, ceramics feature outstanding positive properties because they are usually bio-inert, do not undergo swelling, are chemically and thermally stable, and withstand high mechanical stress enabling the cleaning and reuse of the filter after heat or acid/base

66 treatment for decontamination [10, 11]. These excellent properties result in an increased
67 membrane service life compensating the higher costs of ceramics in comparison to polymeric
68 materials.

69 The most common problem during bacteria filtration is the formation of biofilms on the
70 membrane surface leading to pore clogging and consequently, a reduction of the filter
71 performance is given. These clustered bacterial communities are attached to the membrane
72 surface and protect themselves against environmental influences. Bacteria produce
73 extracellular polymeric substances (EPS) to form complex macroscopic structures that
74 increase their resistance against e.g. toxic chemicals and antimicrobial agents. The removal
75 of biofilms from the membrane surface is challenging and result in both cost- and time-
76 intensive membrane regeneration procedures. Therefore, the reduction of the initial physical
77 attraction of bacteria to the membrane surface, which can be attributed to a reversible
78 attachment [1], plays a key role in inhibiting the formation of biofilms and several antibacterial
79 surfaces have already been proposed [12, 13]. Especially, immobilized nanosilver can act as
80 an efficient antibacterial agent by killing retained bacteria directly on the membrane surface.

81 The decoration of filtration membranes with nanomaterials [14] have come into spotlight for
82 water decontamination, catalysis and environmental remediation exploiting their unique
83 surface chemical activities. Though the use of silver as an antimicrobial agent is known for
84 about 7000 years [15], upcoming with the urgent need to eradicate antibiotic-resistant
85 bacteria and with new insights into the mechanism of action [16], the use of silver has
86 regained an emerged interest along with new interesting fields of applications [17]. Silver
87 displays a broad antibacterial spectrum against Gram-positive and -negative bacteria [18]
88 and nanosilver is one of the safest and mildest antibacterial agents for mammalian cells [19].

89 In recent years, silver nanoparticles (Ag_{nano}) have been embedded into various materials to
90 generate antibacterial composites [20-23] and especially polymeric nanocomposite
91 membranes are produced for water filtration purposes [6, 14, 24-27], since nanoparticles

feature advantages in comparison to bulk silver: i) very small amounts of silver are needed due to the high specific surface area of silver nanoparticles, ii) when compared to silver ions, the bactericidal effect of Ag_{nano} is long-lasting because zerovalent (metallic) Ag_{nano} are not inactivated by complexation and precipitation [28] iii) a controllable release of Ag^{+}-ions from the particles [29] compose them a cost-effective material for surface coatings. Most of the studies investigated the antibacterial properties of the nanocomposite membranes by describing the effect of the physical contact between silver nanoparticles and bacterial cells, but experiments were not performed under filtration conditions with special focus on antibacterial efficiency and silver leaching [27].

In our study, we present an advanced water filtration system based on ceramic capillary membranes which are subsequently doped with Ag_{nano}. Using zirconia as membrane material and Ag_{nano} as bactericidal coating, we combine a promising filtration material exhibiting high fracture toughness and bending strength with a highly effective antibacterial agent. Pore sizes of the capillary membrane of less than 0.2 µm and high open porosities of 51 % enable the retention of bacterial cells during filtration [30]. Generated by direct reduction of silver nitrate on the membrane surface, immobilized Ag_{nano} display a bactericidal surface that kills filtrated bacteria directly on the membrane surface. Filtration experiments were performed by applying intracapillary feeding with bacterial suspensions and bacterial retention after different filtration times was determined using microbiological methods. The viability of retained bacteria was analyzed to evaluate the bactericidal action of immobilized Ag_{nano} and silver leaching during filtration was determined to consider eco-toxicological requirements.

2. MATERIALS AND METHODS

2.1 Preparation of Ag_{nano}-doped zirconia capillaries

Zirconia capillary membranes were fabricated by extrusion and sintered at 1050°C for 2 h as described in our previous study [30]. As shown in Fig. 1, Ag_{nano} were immobilized on the membrane surface by a two-step immersion procedure according to the Creighton method [31] by direct reduction of silver ions on the surface of the capillaries. Capillaries featured an outer diameter (D_O) of 1.48 ± 0.01 mm, an inner diameter (D_I) of 0.90 ± 0.01 mm and an average wall thickness of 0.29 mm ± 0.01 mm. For all further tests, capillary pieces of 25 mm length were used which is in accordance with a weight of 82.9 ± 0.7 mg and a geometric surface area of 189 mm^2, except for the filtration experiment where 100 mm capillaries were applied (geometric surface area of 750 mm^2).

For the immobilization of Ag_{nano} one sintered capillary with a length of 25 mm was immersed in 2 mL silver nitrate ($AgNO_3$) solution (Sigma Aldrich, Germany, Product number 209139) with varying concentrations from 2.5 to 10 mM at 25°C and shaken at 1000 rpm for 5 min (pH was not adjusted). For the reduction of the immobilized silver ions, capillaries were subsequently immersed in 2 mL sodium borohydrate ($NaBH_4$) (Sigma Aldrich, Germany, Product number 209139) for further 5 min. The reduction of the pre-immobilized silver ions was performed using a constant concentration of 2 mM $NaBH_4$. Prior to use, the $NaBH_4$ solution was stirred for 30 min at 25°C followed by a cooling step to 4°C without adjusting the pH. The number of immersion steps was varied between 1, 3, 5 and 10. Afterwards, the capillaries were washed twice in 15 mL of ddH_2O under shaking at 1000 rpm for 5 min to remove unbound and weakly bound silver and finally dried at 70°C for 30 min.

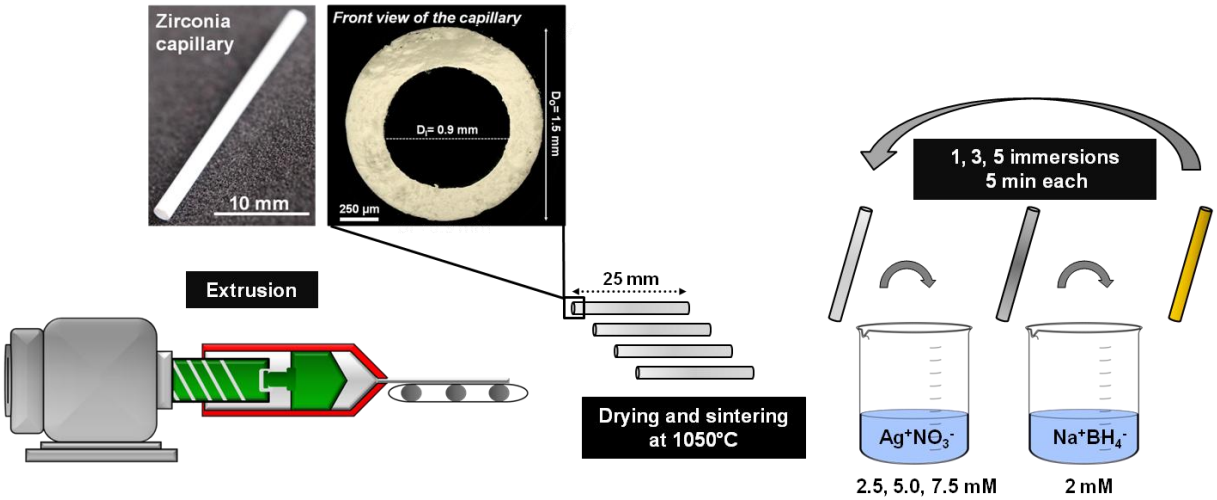

Fig. 1 Synthesis of zirconia capillaries by extrusion and immobilization of Ag_{nano} by reduction of $AgNO_3$ using $NaBH_4$

Zirconia capillaries with an outer diameter (D_O) of 1.48 ± 0.01 mm, an inner diameter (D_I) of 0.90 ± 0.01 mm and an average wall thickness of 0.29 mm ± 0.01 mm were fabricated by extrusion. The extruded capillaries were dried at room temperature for 2 days and the obtained green parts were sintered at 1050°C for 2 h. Silver ions were directly reduced on the surface of the capillary membranes by immersion in $AgNO_3$ solution with varied concentrations and subsequently reduced in $NaBH_4$ at a constant concentration of 2 mM. This two-step immersion procedure was repeated 1-5 times to obtain adequate silver loading capacities.

2.2 Silver loading capacities of Ag_{nano}-capillaries

Silver loading capacities were determined by three different methods: i) manual counting of immobilized Ag_{nano}, ii) image analysis using an image processing algorithm and iii) atomic absorption spectroscopy (AAS).

Scanning electron microscopy (SEM) micrographs of untreated and Ag_{nano}-capillaries were taken with a SEM Supra 40 (Carl Zeiss, Germany) operated at 2 kV. The chemical composition of both the membrane material and immobilized Ag_{nano} was recorded using an energy-dispersive X-ray spectroscopy (EDX) detector (BrukerXFlash 6|30, Bruker Nano GmbH, Germany). The number of immobilized Ag_{nano} on the membrane surface was determined by manual counting using three different SEM micrographs for each membrane sample and four randomly chosen micrograph sections covering an area of 1 µm^2.

Additionally, the micrographs were analyzed using an image processing algorithm called "Silver-Particle Analyzer". The algorithm was developed in C# using Visual Studio 2012 with .NET 3.5 Framework and AForge.NET 1.7.0 Framework. The program used the characteristic gray-value distribution of the Ag_{nano} on the SEM micrographs. The analyses were carried out by screening the SEM images with a so-called top-hat filter. The top-hat filter is applied at a fixed size of 7x7 pixels which can be attributed to the size range of the Ag_{nano}. To consider exclusively the Ag_{nano} and no parts of the porous substrate, the contrast was increased and a threshold value for bright image segments was applied. The algorithm was used to quantify the percentage of Ag_{nano}-covered capillary surface and the total surface of bioactive silver based on the assumption that all Ag_{nano} were spherical. Results were compared with total silver loadings obtained from AAS analysis.

AAS measurements were performed to determine the total amount of immobilized Ag_{nano} on the surface of the capillaries. To quantify the silver loading, one 100 mm Ag_{nano}-capillary was acidified in 10% HNO_3 at 25°C overnight. Due to applied acidic conditions, a complete release of the immobilized silver from the capillaries was enforced. An aliquot of 100 µL of the solution was stored at 4°C until AAS measurements were performed (measurements were performed in triplicate using three individual capillaries). The silver loading was quantified by graphite furnace AAS using an Unicam 989 QZ AA Spectrometer with GF90 plus furnace and FS90 plus autosampler (Unicam, Cambridge, UK) after *aqua regia* digestion. The digestion was carried out by adding 80 µL of concentrated HCl (37 %, p.a. VWR, Germany) and 20 µL of concentrated HNO_3 (≥65 %, puriss p.a., Sigma-Aldrich, Germany) to the samples. After short mixing and centrifugation, the open samples were tempered at 56 °C overnight. The dry residue was dissolved in 1 mL diluted *aqua regia* (containing 10 % HNO_3 and 19 % HCl). Subsequently, the samples were measured after further dilution to be in the working range of the AAS (0.5 – 20 µg Ag L^{-1}).

2.3 Tests on antibacterial properties and filtration efficiencies of Ag_{nano}-capillaries

For all tests, bacterial suspensions of *E. coli* (Deutsche Sammlung von Mikroorganismen und Zellkulturen, Germany, DSMZ No. 1077) were prepared by inoculating a pre-culture in 70 mL of lysogeny broth (LB) (Sigma Aldrich Germany, No. L3022) for 16 h at 37°C to allow a growth until the stationary phase is reached. Bacterial cells were washed once in OECD medium, which is used to simulate realistic surface water conditions [32] and the cell pellet collected by centrifugation was resuspended in OECD medium to obtain a realistic bacterial cell concentration of 10^8 cells/mL for wastewaters [33] according to McFarland standards [34]. Before use, capillaries were heat sterilized at 160°C for 3 h. According to preliminary tests, this sterilization did not affect the bactericidal properties of the capillaries (data not shown).

2.3.1 Agar plate test

Ag_{nano} and untreated capillaries as a reference (each 25 mm length) were separately incubated in 4 mL *E. coli* suspensions at RT and 200 rpm for 30 min. After incubation, the capillaries were briefly washed in OECD medium to remove residual bacterial cells from the inner channel of the capillary (lumen), and subsequently placed on fresh LB plates containing 1.5% (w/w) agar. Incubation of the plates was performed at 37°C for 24 h allowing the bacteria to grow.

2.3.2 Filtration test

Bacterial suspensions of *E. coli* were used for filtration purposes using untreated and Ag_{nano}-capillaries with accessible lengths of 100 mm, respectively. Filtration tests were performed in dead-end mode. Therefore, one end of the capillary was sealed with a two-component polydimethylsiloxane glue (Wirosil®, BEGO, Germany), while the other end of the capillary was connected to a convenient silicon tubing. Four individual capillaries (untreated vs. Ag_{nano}) and independent bacterial cultures were used. For intracapillary feeding with bacterial

suspensions, a peristaltic pump (BVB Standard, Ismatec, Germany) was set to a constant flow rate of 250 µL min^{-1}. Permeates were collected and analyzed regarding the presence of bacterial cells using three different microbiological methods. Adenosin triphosphate was used as an indicator of bacterial metabolism and measured using a luciferase-based cell viability assay as described by Lara et al. [35]. 50 µL of the permeate were mixed with 50 µL of BacTiterGlo Assay (Promega No. G8231, Germany) and luminescence counts, directly correlating with the amount of present ATP, were recorded using a luminescence plate reader (Chameleon V, Hidex, Germany). Furthermore, the optical density of the bacterial suspension at 595 nm ($OD_{595\ nm}$) was measured using a plate reader (Chameleon V, Hidex, Germany). Colony forming units (CFU) were determined by plating the undiluted permeate onto agar plates (Coliform Count Plate, Petrifilm, 3M, Germany) and CFUs were counted after an incubation at 37 °C for 24 h. All experiments involving ATP assay, OD measurements, and CFU tests were performed using three replicates. Obtained results based on permeate samples were compared with those from the bacterial feed solution which were set as 100% survival of bacteria cells.

Preliminary results showed that capillaries stood a bacterial load which was corresponding to a membrane flux reduction of 30%, which was reached after 150 min. Consequently, filtration was stopped after 150 min and back flushing was initiated to remove retained bacterial cells from the inner capillary membrane surface. For this, capillaries were immersed into fresh OECD medium and the peristaltic pump was operated in back flush mode with a membrane flux of 1.27 mL min^{-1} for 1/10 of the filtration time, in this case i.e. 15 min. The back flushed suspension was analyzed by using ATP assay, OD measurement and determination of CFU as described before to determine the bacterial viability of the recovered bacterial cells. The back flushed volume was determined and correlated with the filtration volume of each individual capillary for further calculations.

2.3.3 Silver leaching during filtration

Silver leaching from Ag_{nano}-capillary membranes during filtration was analyzed by determining the silver content of bacteria-free permeate samples via AAS after filtration times of 30 min, 1 h and 2 h, respectively. The filtration conditions (i.e. bacterial feed concentration, buffer, applied flow rate) as well as the length of Ag_{nano}-capillaries were the same compared to the bacterial filtration tests described in chapter 2.3.2. For statistical significance three individual capillary membranes were analyzed and permeate samples were collected on three consecutive days where one filtration cycle was performed per day. After each filtration cycle, back flushing was applied for membrane regeneration. For this, capillaries were immersed into fresh OECD medium and the peristaltic pump was operated in back flush mode with a flow rate of 1.27 mL/min for 1/10 of the filtration time (i.e. 12 min). During the time between back flushing and a new filtration cycle the capillaries were held humid and stored at 4 °C over night to provide stable conditions. For AAS measurements 100 µL of the permeate samples were immediately acidified after filtration by adding 10 µL HNO_3 (1 %) and stored at 4 °C. Afterwards, AAS measurements were performed as described in chapter 2.2 and untreated capillary membranes served as controls for all experiments.

3. RESULTS AND DISCUSSION

3.1. Surface properties of Ag_{nano}-ceramic capillary membranes

Zirconia capillary membranes were fabricated by extrusion as described in our previous work [30] and functionalized with Ag_{nano} in a straightforward two-step procedure via direct reduction of $AgNO_3$ on the capillary surface. As shown in Fig. 2A, the presence of Ag_{nano} on the capillary changed the color of the surface from white (non-functionalized capillary made of zirconia) to yellow indicating a homogeneous surface coating. SEM micrographs demonstrate the presence of homogenously distributed Ag_{nano} on the capillary outer surface

(Fig. 2C), whereas the microstructure of the surface of a non-functionalized capillary is shown in Fig. 2B. EDX analysis confirmed that the immobilized nanoparticles on the membrane surface consisted of silver (Fig. 2C, inset). In addition, SEM micrographs of the inner surface of capillaries produced by using 5 mM $AgNO_3$ and 5 immersion cycles were taken and displayed a similar Ag_{nano} loading (*Supplementary Information*, Figure S1).

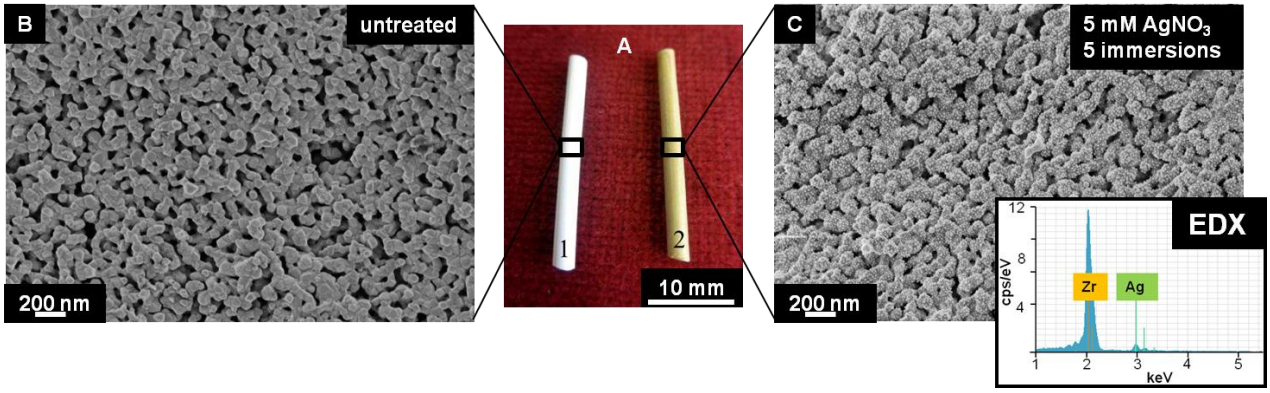

Fig. 2 Untreated and Ag_{nano}-ceramic capillary membranes

Direct formation of Ag_{nano} on the surface of zirconia capillaries leads to a color change from white, displaying the non-functionalized capillary, to yellow (A). Ag_{nano} were generated by 5 immersion cycles using 5 mM $AgNO_3$ and 2 mM $NaBH_4$. SEM micrographs confirm the presence of homogeneously distributed Ag_{nano} on the functionalized capillary (C), whereas the microstructure of a non-functionalized capillary is shown in part B. EDX analysis revealed the presence of silver on the functionalized membrane surface (C, inset).

3.2 Loading capacities of immobilized Ag_{nano} on ceramic capillary membranes

Yielding a high Ag_{nano} loading on the membrane surface, different $AgNO_3$ concentrations in the range between 2.5 and 10 mM and different numbers of immersion cycles (1, 3, 5 and 10 immersions, respectively) were applied, whereas the incubation time (5 min) and the concentration of the reduction solution $NaBH_4$ (2 mM) were held constant. For quantification of immobilized Ag_{nano} on the membrane surface, three different methods were employed: manual counting of Ag_{nano} on randomly chosen sections of SEM micrographs, image analysis of SEM micrographs using the software tool "Silver-Particle Analyzer" and atomic absorption spectroscopy (AAS).

As shown in Fig. 3A, manual counting revealed that the highest loading capacity of 1702 ± 91 Ag_{nano} per μm^2 capillary was achieved when using a 5 mM $AgNO_3$ solution in combination with five successional immersion steps, alternating membrane incubation in $AgNO_3$ solution and in the reduction solution $NaBH_4$. In general, regarding one particular $AgNO_3$ concentration (2.5 mM, 5 mM and 7.5 mM, respectively), increased numbers of immersion steps led to increased numbers of immobilized Ag_{nano}. Compared to an initial $AgNO_3$ concentration of 2.5 mM, Ag_{nano}-doped membranes fabricated by using 5 mM $AgNO_3$ showed higher loading capacities by a factor of 1.3 (one immersion), 5.3 (three immersions) and 5.0 (five immersions), respectively. An increase of the $AgNO_3$ concentration to 7.5 mM did not further increase the Ag_{nano} loading on the membrane and loading capacities were in the same order of magnitude compared to 2.5 mM $AgNO_3$. The application of a higher concentration of 10 mM $AgNO_3$ and 10 immersion cycles led to the undesired formation of agglomerates of immobilized Ag_{nano}, which were inhomogeneously distributed on the capillary surface (data not shown). Providing high Ag_{nano} loadings in combination with a homogeneous membrane surface coating the application of five immersion cycles is the method of choice.

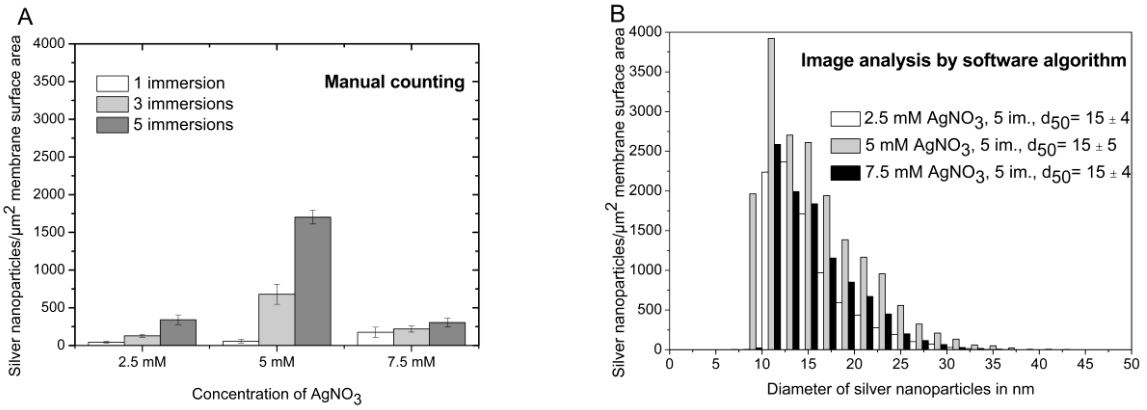

Fig. 3 Quantification of immobilized Ag_{nano} on the capillary surface

Assessment of the number of Ag_{nano} on the surface of the capillary membranes derived from manual counting of four different regions on three different SEM micrographs covering an area of 1 μm^2 each (A). Ag_{nano} size distribution covering an area of 1 μm^2 capillary obtained by image analysis software (B).

Additionally, an image analysis software was applied to quantify the particle size distribution of immobilized Ag_{nano} on the membrane surface (Fig. 3B). Results stood in good correspondence with the results derived from manual counting (Fig. 3A) exhibiting the highest number of Ag_{nano} on capillaries generated by using 5 immersion steps in 5 mM $AgNO_3$ *(*Fig. 3B, *Supplemental Information,* Tab. S1). Silver particle sizes were in the range of approximately 9-35 nm and the average particle diameter for the applied production conditions was calculated to be d_{50} = 15 nm (Fig. 3B) indicating that different $AgNO_3$ concentrations from 2.5 to 7.5 mM lead to similar silver particle sizes and morphologies.

Referring to a geometric surface area of 1 mm^2 on Ag_{nano}-capillaries, the active silver surface on the outer and inner surface of the capillary was calculated to allow an assessment of the total silver surface that can interact with the filtrated bacterial cells. For the calculation based on the particle area that was recognized by the analysis software, it was assumed that all Ag_{nano} were spherical and the contact area between the nanoparticles and the capillary surface was negligible. Again, the highest accessible silver surface area of 0.594 mm^2 was present on capillaries treated with 5 mM $AgNO_3$, whereas capillaries treated with 2.5 mM and 7.5 mM exhibited a total silver surface of 0.269 and 0.314 mm^2, respectively. Implicating the density of silver (10.49 g/cm^3), total amounts of silver were calculated and capillaries treated with 5 mM $AgNO_3$ and 5 immersion steps yielded the highest silver loadings of 20 ng per 1 mm^2 geometric surface area (Tab. 1).

Tab. 1: Accessible silver surface area and total amount of immobilized silver on 1 mm^2 geometric surface area of Ag_{nano}-capillaries

Conditions for the immobilization of silver nanoparticles	Accessible silver surface area in mm^2*	Total amount of silver in ng**
2.5 mM $AgNO_3$, 5 immersions	0.269 ± 0.076	8.23 ± 2.51

5 mM $AgNO_3$, 5 immersions	0.594 ± 0.129	20.00 ± 5.08
7.5 mM $AgNO_3$, 5 immersions	0.314 ± 0.101	9.95 ± 3.90

***The accessible silver surface area was calculated based on software-calculated pixel areas and on the assumption that all Ag_{nano} were spherical.**

**** The total amount of immobilized Ag_{nano} was calculated considering the density of silver (10.49 g/cm^3).**

The two methods, manual counting and software generated particle counts, only consider the Ag_{nano} distribution on the geometric outer and inner surface of the ceramic capillary based on SEM micrographs. The possible penetration of Ag_{nano} into the pores of the membrane material was therefore not considered. With regard to this, we additionally determined the total silver loadings of capillaries treated with 5 mM $AgNO_3$ by AAS. Using this method, an acidic digestion ensured the total release of silver from the capillaries. With regard to the surface of the pores, the measured amounts of total silver loadings were correlated to the specific surface area of Ag_{nano}-capillaries of 7.05 m^2/g *(Supplemental Information,* Table S2). The obtained AAS results were comparable to the results derived from counting: total Ag_{nano} loadings increased with the number of immersions featuring 0.048 ± 0.001 ng silver/mm^2 specific surface area for 1 immersion, 0.123 ± 0.004 ng silver/mm^2 of capillary specific surface area for 3 immersions and 0.176 ± 0.040 ng silver/mm^2 of capillary specific surface area for 5 immersions (Fig. 4 A). It is noticeable that the calculated amount of bioactive silver based on pixel-generated data of 20 ng per 1 mm^2 geometric surface area was significantly higher than the total amount of silver of 0.18 ng per 1 mm^2 specific surface area that was measured via AAS. The discrepancy of the results can be explained by the different reference membrane areas that were applied. Results from the counting method must be referred to the geometric surface area, since only Ag_{nano} on the outer membrane of the capillaries were considered for the counting. Fig. 4B and Fig. C clearly display that Ag_{nano} penetrated to a large extent into the pores of the capillary membrane. For that reason, for the

356 determination of total silver loadings via AAS, the specific surface area determined via
357 nitrogen-adsorption was considered as a reference leading to significantly lower values.
358 Simultaneously, the deep penetration of Ag_{nano} into the pores displays an advantage by
359 enhancing the accessible interaction surface of bactericidal Ag_{nano} and filtrated bacteria.

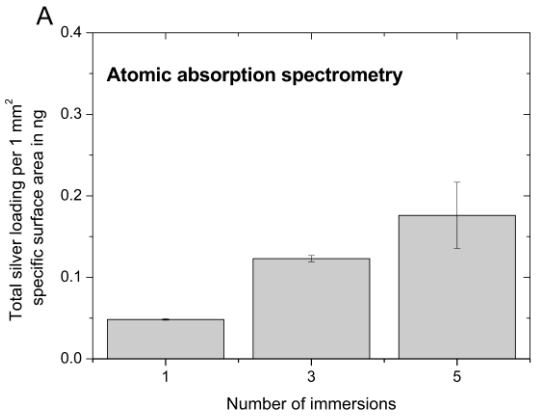

360

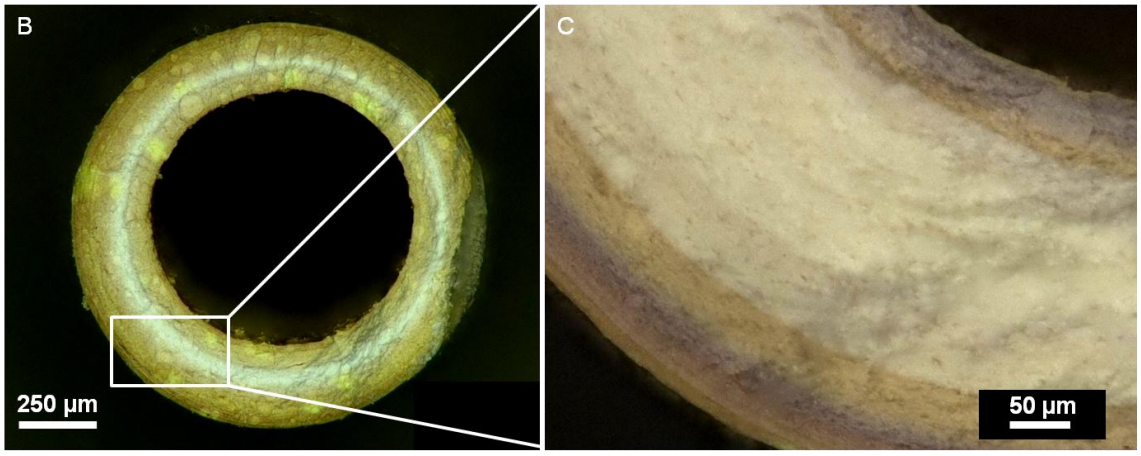

361

362 **Fig. 4: Total amount of immobilized Ag_{nano} per 1 mm^2 specific surface area measured via AAS**
363 **and penetration of immobilized Ag_{nano} into the membrane material (5 mM $AgNO_3$, 5 immersions)**

364 AAS revealed total silver loadings of capillary membranes that were produced using 5 mM $AgNO_3$ and
365 varying numbers of applied immersions (A). Cross section of a Ag_{nano}-doped capillary membrane
366 where the intensity of the yellow coloration is correlated with the content of immobilized silver
367 nanoparticles (B, C).

368

369 Membrane pore size distributions as well as pore volumes and mechanical properties of
370 untreated and Ag_{nano}-capillaries (5 mM $AgNO_3$, 5 immersion steps) were determined by
371 nitrogen adsorption isotherms (BET-BJH evaluation) and bending strength tests (3-point

bending test). Results showed that the additional Ag_{nano}-functionalization did not significantly alter both, the membrane pore sizes and the mechanical properties of the zirconia capillaries [30] providing an efficient filtration performance and good mechanical properties for handling purposes *(Supplemental Information,* Table S2, Figure S2).

3.3 Bactericidal properties of Ag_{nano}-capillaries under batch and filtration conditions

Bactericidal properties of Ag_{nano}-capillaries were analyzed by incubating untreated and Ag_{nano}-capillaries in bacterial suspensions of *E. coli* for 30 min at room temperature. As expected, bacterial growth was only visible close to the untreated capillaries, whereas Ag_{nano}-capillaries prevented the growth of *E. coli* cells displaying significant bactericidal properties (Fig. 5).

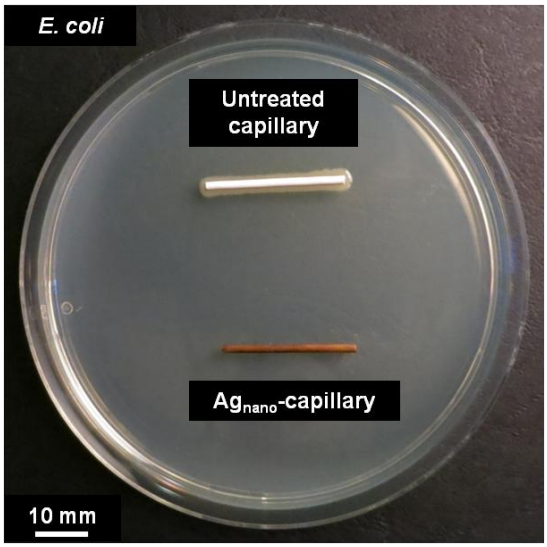

Fig. 5 Bactericidal properties of Ag_{nano}-capillary membranes

An agar plate test displays the bactericidal properties of the Ag_{nano}-capillaries (5 mM $AgNO_3$, 5 immersion cycles) against Gram-negative *E. coli*. While considerable bacterial growth was observed close to the untreated capillaries, the Ag_{nano}-capillaries exhibited no bacterial growth.

For realistic fresh water filtration conditions the standardized OECD medium was chosen for the preparation of the bacterial feed, since it is used for experiments with the freshwater algae *Pseudokirchneriella subcapitata* [36]. Filtration of an *E. coli* suspension was performed in dead-end mode by intracapillary feeding at an initial flow rate of 250 µL/min for 2.5 h using

100 mm capillaries (exhibiting a geometric surface area of 750 mm^2) and the resulting permeates of untreated and Ag_{nano}-capillaries were analyzed every 30 min regarding bacterial viability by measuring ATP levels, CFU and OD_{595nm}. Results showed highly efficient filtration efficiencies for untreated and Ag_{nano}-capillaries achieving a bacterial retention of nearly 100 % which corresponds to a log_{10} reduction value (LRV) of 8 (Fig. 6 A, B). No CFUs were detected after plating the permeate samples onto agar plates and ATP and OD_{595nm} levels of the permeate samples were comparable to the buffer controls indicating a clear and bacteria-free solution (data not shown). Achieving log_{10} reduction levels of >6, the here presented capillaries accomplish the bacteria filter criterion for safe and clean drinking water according to the U.S. Environmental Protection Agency [37].

Since the membrane flux decreased during filtration, back flushing was induced for membrane regeneration after the filtration of approximately $3x10^9$ bacterial cells per capillary (750 mm^2 geometric surface area), which corresponds to a filtration time of 2.5 h. Back flushing was applied for 1/10 of the filtration time and filtration efficiencies were recovered by reaching 95-100% of the initial membrane flux (Fig. 6 A, B).

Since both, untreated and Ag_{nano}-capillaries, featured similar filtration properties, the assumed benefit of the Ag_{nano}-immobilization is the inhibition of the initial attachment of living bacteria [38, 39] to the capillary surface and the inhibition of initial biofilm formation. In general, after initial attachment, bacteria start to secrete extracellular polymeric substances providing a matrix for other bacteria to embed and build a biofilm [40]. This biofilm leads to pore blocking which is followed by an increase of the transmembrane pressure and operating time leading to lower filtration efficiencies. Creating a strong bactericidal surface by using an Ag_{nano} coating, bacteria are assumed to die when coming into contact with the capillary membrane before the expression of biofilm components will be initiated and dead bacteria will be removed by operating the pump in back flush mode [41].

418 To analyze the viability of the retained bacteria, the recovered bacteria from back flushing
419 were analyzed regarding ATP levels and CFU. Unfortunately, bacteria that were recovered
420 from Ag_{nano}-capillaries during back flushing after 150 min filtration were found to be viable as
421 measured by ATP levels and CFU. The amount of filtrated bacteria was probably too high so
422 that the contact of bacterial cells with the bactericidal Ag_{nano} surface could not be assured
423 (data not shown).

424 Therefore, individual Ag_{nano}-capillaries were tested for filtration times of 30, 60, 90, 120 and
425 150 min to identify the maximum filtration time that ensured the death of retained bacteria.
426 Back flushing after 30 min and 60 min filtration time showed that recovered *E. coli* cells from
427 Ag_{nano}-capillaries were dead displaying marginal bacterial ATP levels of 3.4 and 1.6 % in
428 comparison to reference bacteria that were recovered from untreated capillaries (Fig. 6C).
429 Capillaries that were used for longer filtration times of >60 min were not capable in killing
430 bacterial cells at the inner membrane surface of the capillaries as shown by determined ATP
431 levels (Fig. 6C). Back flushing of Ag_{nano}-capillaries should therefore be initiated after a
432 maximum filtration time of 60 min, corresponding to a bacterial load of $6x10^8$ bacterial
433 cells/750 mm^2 geometric capillary surface area.

434 Understanding the stability of each individual bactericidal Ag_{nano} membrane coating, Ag_{nano}-
435 capillary membranes were tested for five consecutive filtration cycles of 60 min each, while
436 back flushing was initiated after each cycle. Microbiological results showed that bacterial
437 viability was decreased to 2-5 % in relation to the reference bacteria that were recovered
438 from untreated capillary membranes as analyzed by ATP levels and CFU indicating a stable
439 bactericidal membrane surface at suitable filtration times of 60 min (Fig. 6D).

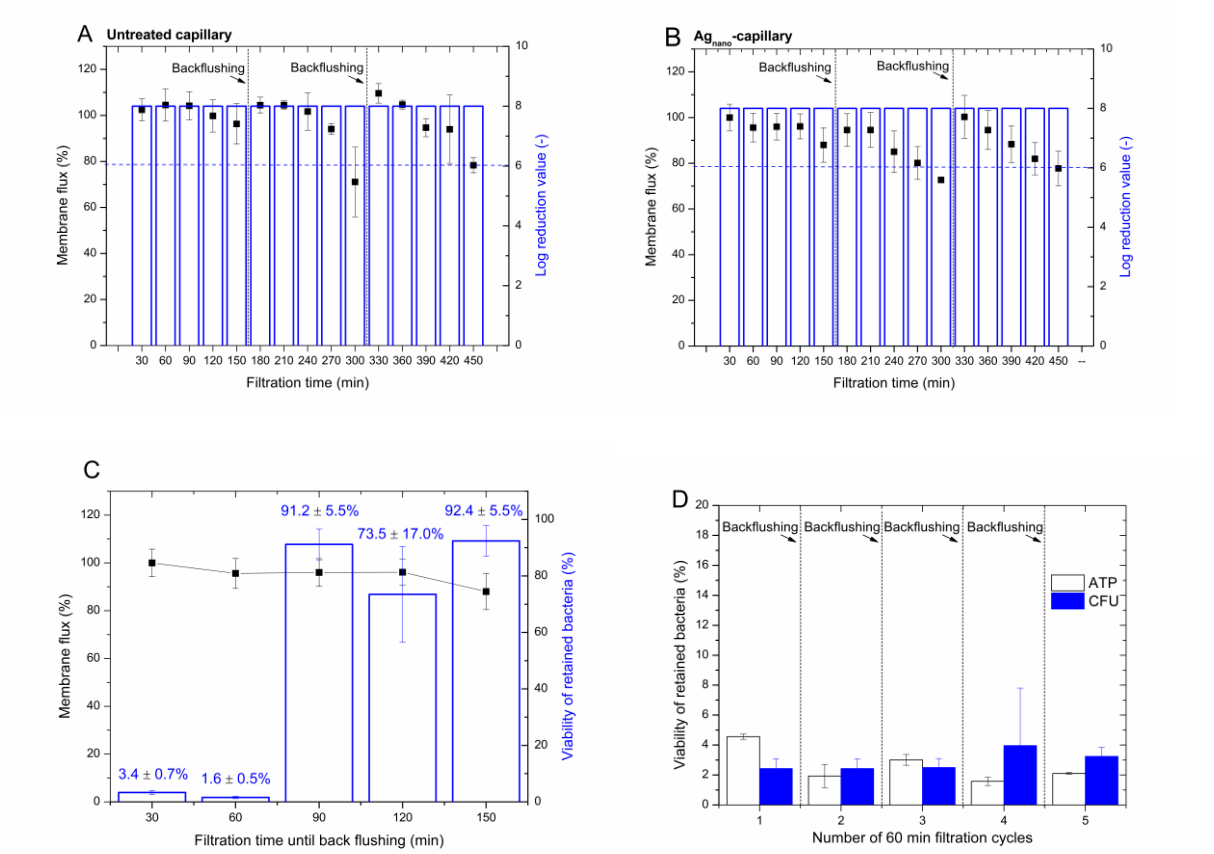

Fig. 6 Filtration efficiencies of untreated and Ag$_{nano}$- capillaries

Filtration in dead-end mode by intracapillary bacterial feeding was performed using untreated (A) and Ag$_{nano}$-capillary membranes (B) resulting in bacterial retention values of $\log_{10}$ 8. The blue, dashed line indicates the requirements on safe and clean drinking water of log reduction values of 6 according to the U.S. Environmental Protection Agency. Back flushing was applied after a filtration time of 2.5 h, corresponding to approximately 3x10^9 cells, resulting in regained membrane fluxes of 95-100%. No significant differences in bacterial retention rates ensuring log reduction values of 8 were obtained for untreated versus Ag$_{nano}$-capillary membranes (A, B).

Individual Ag$_{nano}$-capillaries were used for different filtration times to identify the maximum filtration time that still guaranteed the killing of retained bacteria: filtration times of ≤60 min allowed the killing of filtrated bacteria (C). Regarding the stability of the bactericidal membrane coating, Ag$_{nano}$-capillaries were efficient in killing retained bacteria after five consecutive filtration cycles of 60 minutes each, where back flushing was applied for membrane regeneration (D).

Similar results were obtained by Liu et al. [20] showing that a silver-nanoparticle-decorated polysulfone membranes exhibited anti-adhesiv properties in comparison to unfunctionalized polysulfone membranes. Although the authors reported similar retention rates for unfunctionalized and silver-functionalized polysulfone membranes, significantly more bacteria were detached during rinsing experiments from the silver-decorated membranes than from untreated membranes. However, our back flushing results (Fig. 6C) also showed

462 that longer filtration times >60 min were not recommendable, since bacterial killing was not
463 ensured anymore. The bacterial filter cake was probably too thick to allow a contact-induced
464 killing of bacteria by Ag_{nano}.

465 Silver contamination of water is an environmental predicament. Since silver is proved to be
466 toxic against several freshwater organisms such as *Daphnia magna* [42] and may lead to
467 safety concerns [43], its release into the environment needs to be accurately monitored.

468 Thus, the release of silver from the Ag_{nano}-capillaries during filtration and silver maximum
469 contaminant levels were determined. Therefore, samples from the filtrated permeates of
470 three individual capillaries were removed after 30 min, 60 min and 120 min of filtration on
471 three consecutive days and analyzed by AAS. AAS measurements revealed that the silver
472 release was highest at the beginning of the filtration on each individual day. After the first
473 burst release after 30 min of filtration on the first day where 400 ± 3 µg/L of silver were
474 released, silver leaching progressively decreased reaching values of 34 ± 0 µg/L already
475 after 60 min of filtration and only 21 ± 17 µg/L at the last measurement after 420 min of
476 filtration (Fig. 7). Among the filtration cycles, capillaries were stored under humid conditions
477 at 4°C overnight until filtration was started again. The storage induced a continuous release
478 of silver from the capillary, which was then released at the following filtration cycles, which
479 explains the recurring increases of silver release in the beginning of each filtration cycle.
480 High standard deviations result from the phenomenon that small pieces of the capillaries got
481 lost and were measured in the permeate samples. The maximum contaminant level for silver
482 in drinking water is 50 µg/L as set by the World Health Organization (WHO), whereas “under
483 special situations where silver salts are used to maintain the bacteriological quality of
484 drinking-water higher levels of up to 100 µg/L can be tolerated without risk to health” [44].
485 Although silver was continuously released during filtration, WHO requirements were fulfilled
486 already after 1 h of filtration when silver contaminant levels of 34 ± 0 µg/L were reached.

In addition to the eco-toxicological aspect, the loss of the bactericidal coating displays a drawback, because it reduces the operating time and requires a frequent replacement of the coating or the complete membrane. Total silver loading capacities of Ag_{nano}-capillaries of 411.64 ± 94.88 µg silver/100 mm capillary were determined by AAS. The filtration experiment showed that 0.23 ± 0.05 % of the initial silver loading were released after the first 30 minutes of filtration and amounts of 0.01 ± 0.05 % were released after 420 minutes of filtration on the third day. The total silver release during the three-day experiment was determined to be 0.81 ± 0.43 % of the initial silver content that was immobilized on each capillary displaying a very good stability of the bactericidal Ag_{nano} coating.

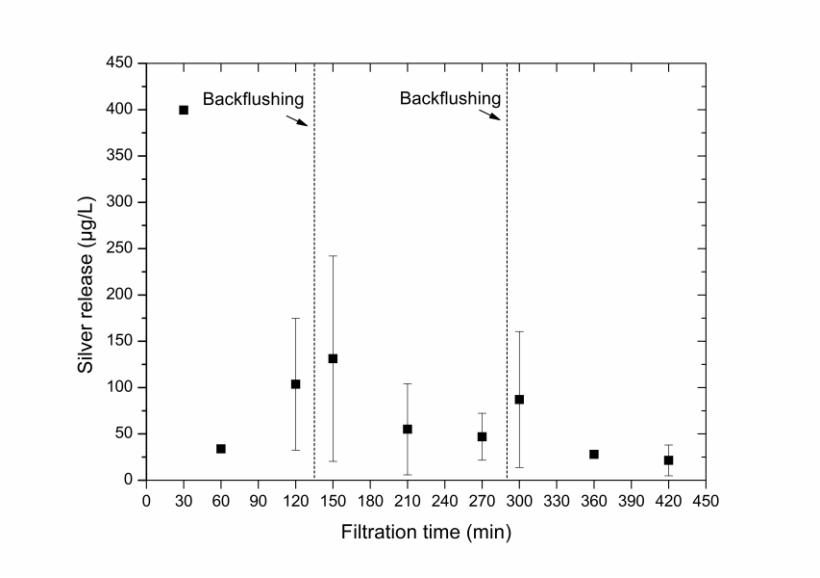

Fig. 7 Silver release during filtration

Silver contents in the permeate samples of three individual capillaries of 100 mm lengths were analyzed using AAS to determine the silver release from the Ag_{nano}-capillaries. For this, permeate samples were removed after 30 min, 60 min and 120 min of filtration on three consecutive days. Silver leaching was highest at the beginning of the three filtration cycles and decreased progressively during each filtration cycle.

Leaching of immobilized silver has also been demonstrated by Chou et al. [45] who analyzed the stability of an Ag_{nano} coating on cellulose acetate hollow fiber membranes. A 180 days static immersion in water decreased the silver content on the membrane surface by 90%, but still an antibacterial effect against *E. coli* and *S. aureus* was evident. In contrast, after

permeating with water for 5 days, a significant higher and faster loss of silver was determined and no antibacterial effect was measurable anymore. Others studies also reported rapid depletions of silver from membrane surfaces after relatively short filtration periods (0.4 L/cm^2) and the soon loss of antibacterial and antiviral activities [6]. The here presented capillaries were capable of killing bacteria during filtration for at least five consecutive filtration cycles of 60 min and the silver release from the membrane after the first 30 min of filtration fulfilled the requirements on eco-toxicological demands.

5. CONCLUSIONS

Porous ceramic capillaries made of zirconia were functionalized with broadband bactericidal Ag_{nano} for utilization as small-sized water purification modules exhibiting durable antibacterial properties. The immobilization of Ag_{nano} was performed via direct reduction of silver nitrate to metallic Ag_{nano} on the surface of the capillaries. This straightforward procedure led to high silver loadings of up to 1700 Ag_{nano} per µm^2 capillary surface when using 5 mM $AgNO_3$ and 5 immersion cycles and could also be transferred to other oxide and non-oxide ceramics, such as aluminum oxide or silicon carbide. Total silver loadings as determined by AAS were found to be 0.18 ng silver per 1 mm^2 specific surface area and 20 ng silver per 1 mm^2 geometric surface area as calculated based on nanoparticle-covered membrane surface areas.

Zirconia capillaries exhibited excellent filtration performances obtaining bacterial retention rates of log_{10} reduction values of 8. Back flushing cycles of 1/10 of the filtration time were suggested for membrane regeneration leading to regained filtration efficiencies of 95-100 %.

Creating a strong bactericidal surface, immobilized Ag_{nano} on the zirconia surface efficiently killed bacteria during filtration for filtration times of up to 60 min corresponding to 6x10^8 filtrated bacterial cells/750 mm^2 capillary surface. A subsequent back flushing cycle ensured

the removal of dead cells from the membrane surface leading to the regeneration of filtration efficiencies and allowed the application for consecutive filtration cycles. Release of silver during filtration was analyzed and was moderate leading to silver contaminant levels of 34 µg/L after one hour of filtration (250 µL/min).

Displaying strong bactericidal properties, the described ceramic-silver composite might be beneficial for several disinfection strategies, for example when applied for the coating of medical devices or for areas in which germ-free surfaces are necessary.

Acknowledgements

Financial support from Federal Ministry of Education and Research (BMBF, support code 0315520) is gratefully acknowledged. We thank Petra Witte (University of Bremen, Department of Geosciences) for her support with the SEM.

SUPPLEMENTAL INFORMATION

1) Silver nanoparticle loading capacities on capillary membranes

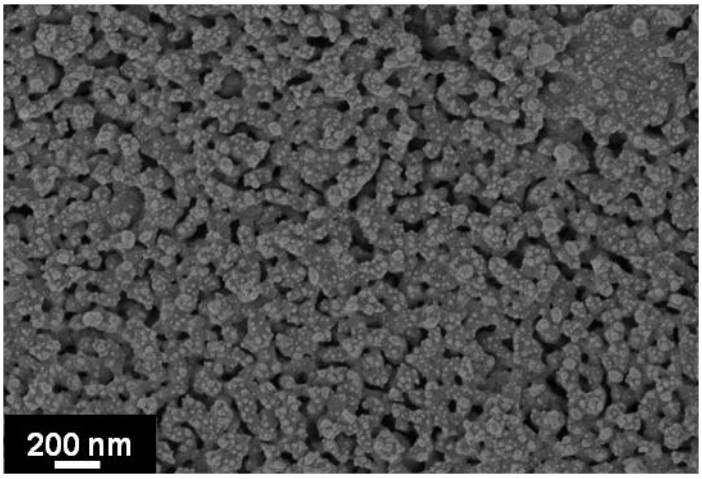

Fig. S1: SEM micrograph of the inner surface of a capillary produced by using 5 mM $AgNO_3$ and 5 immersion steps.

552 **Tab. S1: Ag_{nano} loadings obtained by image analysis software for capillaries produced using**
553 **2.5 mM, 5.0 mM and 7.5 mM $AgNO_3$ and 1, 3 and 5 immersion steps**

Silver nanoparticles/µm² membrane surface area	**2.5 mM $AgNO_3$**	**5 mM $AgNO_3$**	**7.5 mM $AgNO_3$**
1 immersion	147 ± 82	93 ± 83	276 ± 78
3 immersions	371 ± 148	1069 ± 42	1110 ± 417
5 immersions	466 ± 807	2652 ± 741	759 ± 394

554

555 ***2) Porosity and mechanical properties of Ag_{nano}- and untreated capillaries***

556 *Materials and Methods: Pore size distribution, pore volume and specific surface area*

557 The pore size distribution, pore volume and specific surface area of the untreated and Ag_{nano}-
558 doped capillaries were calculated from nitrogen adsorption isotherms according to the
559 method of Brunauer et al. (BET) [46]. Adsorption isotherms have been recorded at -196°C
560 and the calculation of the specific surface areas was performed using a BELSORP-mini (BEL
561 Japan Inc., Japan) and the provided software (BELMaster). All samples were vacuum dried
562 at <0.5 mbar and 120°C for 2 h prior to BET analysis.

563 *Material and Methods: Mechanical strength*

564 According to DIN EN 843-1 the mechanical strength of Ag_{nano}-doped capillaries compared to
565 non-functionalized capillaries (reference) was obtained by three-point bending tests (Roell
566 Z005, Zwick). These measurements were performed using a Zwick Z005 testing machine
567 provided with a load cell for 5 kN (piezoelectric force sensor). The capillary sample (25 mm
568 length) was placed into the centre of a sample holder featuring an 8 mm distance between
569 the support rollers. The bending strength σ_F was calculated as described in our previous

study [30]. 30 samples for each series were tested to achieve a significant average bending strength.

Results: Porosity and mechanical properties of Ag_{nano}- and untreated capillaries

The total pore volume of untreated capillaries of 0.07 ± 0.01 $cm^3\ g^{-1}$ differed markedly from Ag_{nano}-capillaries showing a significant higher total pore volume of 0.12 ± 0.01 $cm^3\ g^{-1}$, while the specific surface area was similar for both samples (7.05 $m^2\ g^{-1}$ versus 8.08 $m^2\ g^{-1}$). The mechanical properties were expected not to be altered after immobilization with Ag_{nano} and three-point bending tests revealed similar bending strengths of 48.1 MPa for untreated and 53.5 MPa for Ag_{nano}-capillaries with relatively high Weibull modules of 14.2 and 8.0, respectively (Tab. S2). Therefore, silver-doping did not alter the membrane properties leading to promising candidates for sustainable bacterial filtration if a sufficient antibacterial activity is achieved.

Figure S2 presents the pore size distributions of untreated (A) and Ag_{nano} (B) capillary membranes determined by BET-BJH. Untreated and Ag_{nano}-capillaries exhibited the same pore size range of 24-196 nm, whereas the median pore size was 80 nm for untreated and 100 nm for Ag_{nano}-capillaries.

Tab. S2: Membrane properties of untreated and Ag_{nano}-capillaries

BET analysis and three-point bending tests revealed similar membrane properties of untreated and Ag_{nano}-capillaries displaying optimal properties for aspired bacterial filtration with median pore sizes of 80 and100 nm and a sufficient mechanical stability showing bending strength values of ~50 MPa.

	Untreated capillary	**Ag_{nano}-capillary 5 mM $AgNO_3$ 5 immersions**
Pore diameter in nm	24-196*	24-196*
Median pore diameter (d_{50}) in nm	80	100
Total pore volume in cm^3g^{-1}	0.07 ± 0.01	0.12 ± 0.01

Specific surface area in m^2g^{-1}	7.05 ± 0.20	8.08 ± 1.04
Bending strength σ_0 in MPa	48.1	53.5
Weibull modulus m (-)	14.2	8.0
(Maximum likelihood)		

*Pore size distributions were determined according to BET-BJH evaluation and upper detection limit was set to 196 nm.

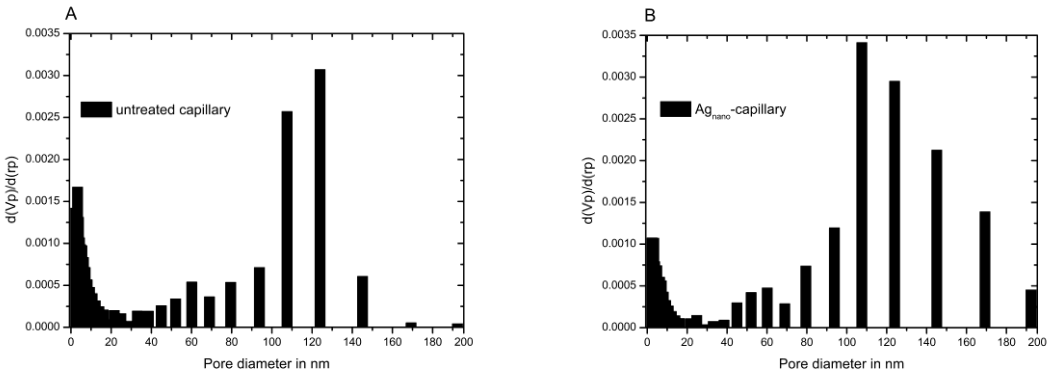

Fig. S2: Pore size distribution of untreated (A) and Ag_{nano}-capillaries (B) determined by nitrogen adsorption isotherms (BET-BJH evaluation)

References

[1] C. Beloin, A. Roux, J.M. Ghigo, Escherichia coli biofilms, Curr Top Microbiol, 322 (2008) 249-289.

[2] E. Butler, A. Silva, K. Horton, Z. Rom, M. Chwatko, A. Havasov, J.R. McCutcheon, Point of use water treatment with forward osmosis for emergency relief, Desalination, 312 (2013) 23-30.

[3] P. Jain, T. Pradeep, Potential of silver nanoparticle-coated polyurethane foam as an antibacterial water filter, Biotechnology and Bioengineering, 90 (2005) 59-63.

[4] J.E. Rademan, Patent: Combinations of liquid filtration media and methods for enhanced filtration of selected water contaminants, RH Black-US Patent 20,130,022,686, (2013).

[5] C.X. Liu, D.R. Zhang, Y. He, X.S. Zhao, R. Bai, Modification of membrane surface for anti-biofouling performance: Effect of anti-adhesion and anti-bacteria approaches, J Membrane Sci, 346 (2010) 121-130.

[6] K. Zodrow, L. Brunet, S. Mahendra, D. Li, A. Zhang, Q.L. Li, P.J.J. Alvarez, Polysulfone ultrafiltration membranes impregnated with silver nanoparticles show improved biofouling resistance and virus removal, Water Res., 43 (2009) 715-723.

[7] P.O. Rujitanaroj, N. Pimpha, P. Supaphol, Preparation, Characterization, and Antibacterial Properties of Electrospun Polyacrylonitrile Fibrous Membranes Containing Silver Nanoparticles, J. Appl. Polym. Sci., 116 (2010) 1967-1976.

[8] S. Liang, G. Qi, K. Xiao, J. Sun, E.P. Giannelis, X. Huang, M. Elimelech, Organic fouling behavior of superhydrophilic polyvinylidene fluoride (PVDF) ultrafiltration membranes functionalized with

surface-tailored nanoparticles: Implications for organic fouling in membrane bioreactors, J Membrane Sci, 463 (2014) 94-101.
[9] A.L. Ahmad, A.A. Abdulkarim, B.S. Ooi, S. Ismail, Recent development in additives modifications of polyethersulfone membrane for flux enhancement, Chem Eng J, 223 (2013) 246-267.
[10] I. Voigt, J. Adler, M. Weyd, R. Kriegel, Ceramic Filters and Membranes, in: Ceramics Science and Technology, Wiley-VCH Verlag GmbH & Co. KGaA, 2013, pp. 117-167.
[11] S. Kroll, M. Oliveira, C. de Moura, F. Meder, G. Grathwohl, K. Rezwan, High virus retention mediated by zirconia microtubes with tailored porosity, J Eur Ceram Soc, 32 (2012) 4111-4120.
[12] L. Treccani, M. Maiwald, V. Zollmer, M. Busse, G. Grathwohl, K. Rezwan, Antibacterial and Abrasion-Resistant Alumina Micropatterns, Adv. Eng. Mater., 11 (2009) B61-B66.
[13] C. Sengstock, M. Lopian, Y. Motemani, A. Borgmann, C. Khare, P.J.S. Buenconsejo, T.A. Schildhauer, A. Ludwig, M. Koller, Structure-related antibacterial activity of a titanium nanostructured surface fabricated by glancing angle sputter deposition, Nanotechnology, 25 (2014).
[14] A. Ananth, G. Arthanareeswaran, A.F. Ismail, Y.S. Mok, T. Matsuura, Effect of bio-mediated route synthesized silver nanoparticles for modification of polyethersulfone membranes, Colloids and Surfaces A: Physicochemical and Engineering Aspects, 451 (2014) 151-160.
[15] S. Chernousova, M. Epple, Silver as Antibacterial Agent: Ion, Nanoparticle, and Metal, Angewandte Chemie International Edition, 52 (2013) 1636-1653.
[16] J.R. Morones-Ramirez, J.A. Winkler, C.S. Spina, J.J. Collins, Silver Enhances Antibiotic Activity Against Gram-Negative Bacteria, Science Translational Medicine, 5 (2013) 190ra181.
[17] S. Zhang, G. Qiu, Y.P. Ting, T.-S. Chung, Silver–PEGylated dendrimer nanocomposite coating for anti-fouling thin film composite membranes for water treatment, Colloids and Surfaces A: Physicochemical and Engineering Aspects, 436 (2013) 207-214.
[18] C.N. Lok, C.M. Ho, R. Chen, Q.Y. He, W.Y. Yu, H.Z. Sun, P.K.H. Tam, J.F. Chiu, C.M. Che, Proteomic analysis of the mode of antibacterial action of silver nanoparticles, J Proteome Res, 5 (2006) 916-924.
[19] A. Melaiye, W.J. Youngs, Silver and its application as an antimicrobial agent, Expert Opin Ther Pat, 15 (2005) 125-130.
[20] Y. Liu, E. Rosenfield, M. Hu, B. Mi, Direct observation of bacterial deposition on and detachment from nanocomposite membranes embedded with silver nanoparticles, Water Res., 47 (2013) 2949-2958.
[21] A. Nguyen, L. Zou, C. Priest, Evaluating the antifouling effects of silver nanoparticles regenerated by TiO2 on forward osmosis membrane, J Membrane Sci, 454 (2014) 264-271.
[22] S. Ghosh, R. Kaushik, K. Nagalakshmi, S.L. Hoti, G.A. Menezes, B.N. Harish, H.N. Vasan, Antimicrobial activity of highly stable silver nanoparticles embedded in agar-agar matrix as a thin film, Carbohyd Res, 345 (2010) 2220-2227.
[23] C. Durucan, B. Akkopru, Effect of Calcination on Microstructure and Antibacterial Activity of Silver-Containing Silica Coatings, J. Biomed. Mater. Res. Part B, 93B (2010) 448-458.
[24] D.Y. Koseoglu-Imer, B. Kose, M. Altinbas, I. Koyuncu, The production of polysulfone (PS) membrane with silver nanoparticles (AgNP): Physical properties, filtration performances, and biofouling resistances of membranes, J Membrane Sci, 428 (2013) 620-628.
[25] H. Basri, A.F. Ismail, M. Aziz, Polyethersulfone (PES)-silver composite UF membrane: Effect of silver loading and PVP molecular weight on membrane morphology and antibacterial activity, Desalination, 273 (2011) 72-80.
[26] J. Huang, G. Arthanareeswaran, K.S. Zhang, Effect of silver loaded sodium zirconium phosphate (nanoAgZ) nanoparticles incorporation on PES membrane performance, Desalination, 285 (2012) 100-107.
[27] M. Sile-Yuksel, B. Tas, D.Y. Koseoglu-Imer, I. Koyuncu, Effect of silver nanoparticle (AgNP) location in nanocomposite membrane matrix fabricated with different polymer type on antibacterial mechanism, Desalination, 347 (2014) 120-130.

669 [28] S. Silver, L.T. Phung, G. Silver, Silver as biocides in burn and wound dressings and bacterial
670 resistance to silver compounds, J Ind Microbiol Biot, 33 (2006) 627-634.
671 [29] Y.H. Lv, H. Liu, Z. Wang, S.J. Liu, L.J. Hao, Y.H. Sang, D. Liu, J.Y. Wang, R.I. Boughton, Silver
672 nanoparticle-decorated porous ceramic composite for water treatment, J Membrane Sci, 331 (2009)
673 50-56.
674 [30] S. Kroll, L. Treccani, K. Rezwan, G. Grathwohl, Development and characterisation of
675 functionalised ceramic microtubes for bacteria filtration, J Membrane Sci, 365 (2010) 447-455.
676 [31] J.A. Creighton, C.G. Blatchford, M.G. Albrecht, Plasma Resonance Enhancement of Raman-
677 Scattering by Pyridine Adsorbed on Silver or Gold Sol Particles of Size Comparable to the Excitation
678 Wavelength, J Chem Soc Farad T 2, 75 (1979) 790-798.
679 [32] J.E. Doe, R.W. Lewis, P.A. Botham, Comments on A Scientific and Animal Welfare Assessment of
680 the OECD Health Effects Test Guidelines for the Safety Testing of Chemicals Under The European
681 Union REACH System, Atla-Altern Lab Anim, 34 (2006) 111-114.
682 [33] D.E. Reisner, Biotechnology II: Global Prospects, (2011).
683 [34] J. McFarland, The nephelometer: an instrument for estimating the numbers of bacteria in
684 suspensions used for calculating the opsonic index and for vaccines, J Amer Med Assoc, 49 (1907).
685 [35] H.H. Lara, N.V. Ayala-Nunez, L.D.I. Turrent, C.R. Padilla, Bactericidal effect of silver nanoparticles
686 against multidrug-resistant bacteria, World J Microb Biot, 26 (2010) 615-621.
687 [36] V. Aruoja, H.-C. Dubourguier, K. Kasemets, A. Kahru, Toxicity of nanoparticles of CuO, ZnO and
688 TiO2 to microalgae Pseudokirchneriella subcapitata, Sci Total Environ, 407 (2009) 1461-1468.
689 [37] U.S.E.P. Agency, Safe Drinking Water Act,
690 http://water.epa.gov/lawsregs/rulesregs/sdwa/filterbackwash.cfm, download 19/07/2013 (2013).
691 [38] J. Hasan, R.J. Crawford, E.P. Ivanova, Antibacterial surfaces: the quest for a new generation of
692 biomaterials, Trends in Biotechnology, 31 (2013) 295-304.
693 [39] D. Inbakandan, C. Kumar, L.S. Abraham, R. Kirubagaran, R. Venkatesan, S.A. Khan, Silver
694 nanoparticles with anti microfouling effect: A study against marine biofilm forming bacteria, Colloids
695 and Surfaces B: Biointerfaces, 111 (2013) 636-643.
696 [40] H.C. Flemming, T.R. Neu, D.J. Wozniak, The EPS matrix: The "House of Biofilm cells", J Bacteriol,
697 189 (2007) 7945-7947.
698 [41] P. Paul, Development and Testing of a Fully Adaptable Membrane Bioreactor Fouling Model for a
699 Sidestream Configuration System, Membranes, 3 (2013) 24-43.
700 [42] S. Asghari, S.A. Johari, J.H. Lee, Y.S. Kim, Y.B. Jeon, H.J. Choi, M.C. Moon, I.J. Yu, Toxicity of
701 various silver nanoparticles compared to silver ions in Daphnia magna, J Nanobiotechnol, 10 (2012).
702 [43] J. Kim, B. Van der Bruggen, The use of nanoparticles in polymeric and ceramic membrane
703 structures: Review of manufacturing procedures and performance improvement for water
704 treatment, Environ. Pollut., 158 (2010) 2335-2349.
705 [44] W.H. Organization, Guideline for Drinking-water Quality – Silver in Drinking water,
706 http://www.who.int/water_sanitation_health/dwq/chemicals/silver.pdf, download 17/06/2013
707 (2003).
708 [45] W.L. Chou, D.G. Yu, M.C. Yang, The preparation and characterization of silver-loading cellulose
709 acetate hollow fiber membrane for water treatment, Polymers for Advanced Technologies, 16 (2005)
710 600-607.
711 [46] S. Brunauer, P.H. Emmett, E. Teller, Adsorption of gases in multimolecular layers, J Am Chem
712 Soc, 60 (1938) 309-319.

713

714

Figure 1

Click here to download high resolution image

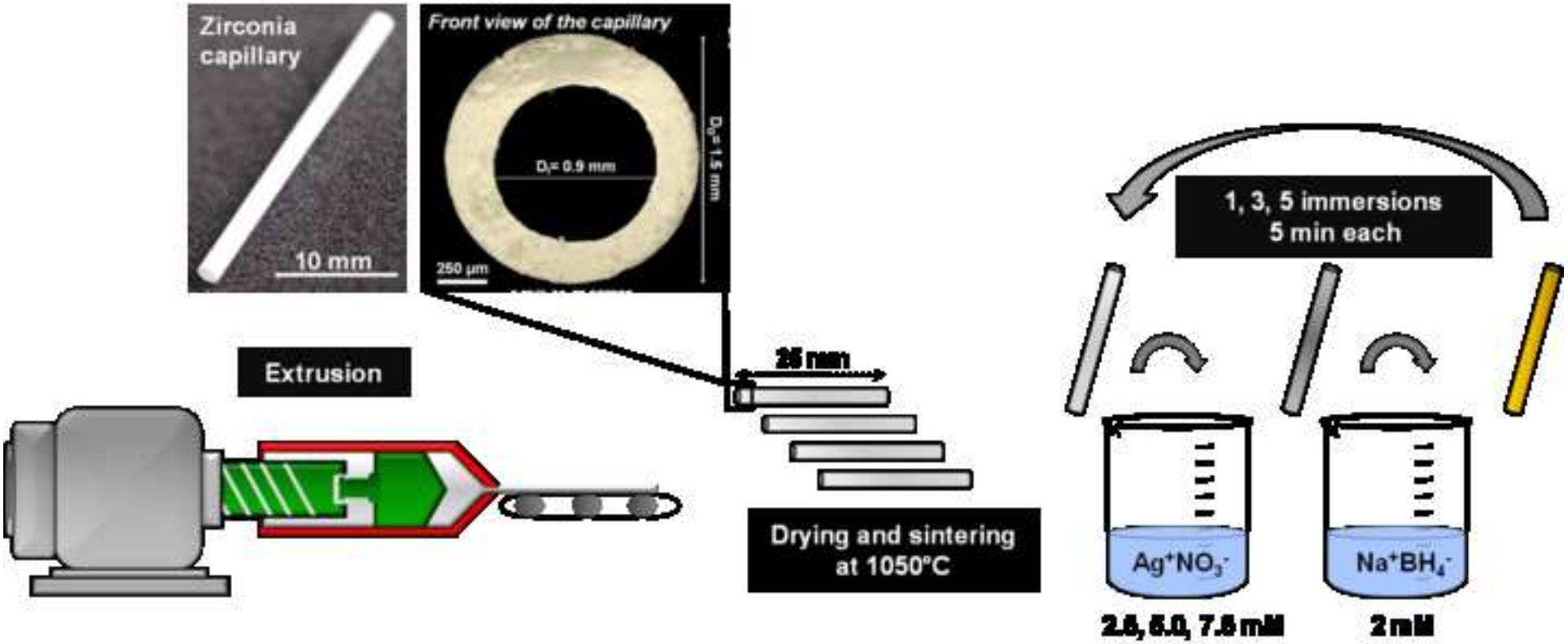

Figure 2A-C

Click here to download high resolution image

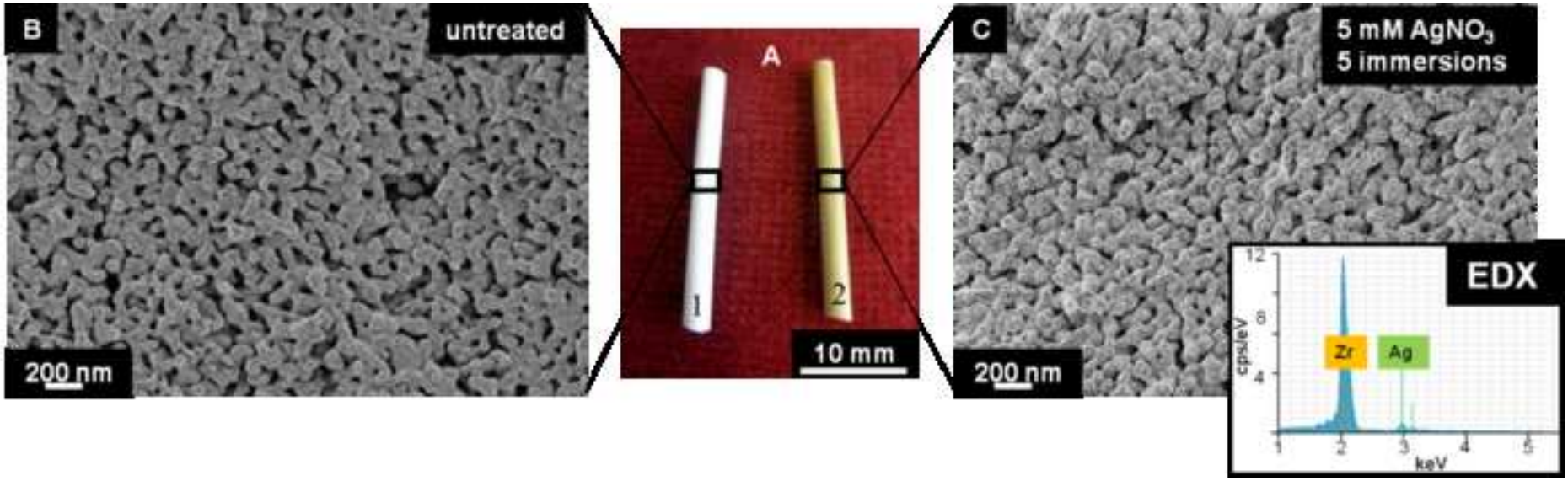

Figure 3A

Click here to download high resolution image

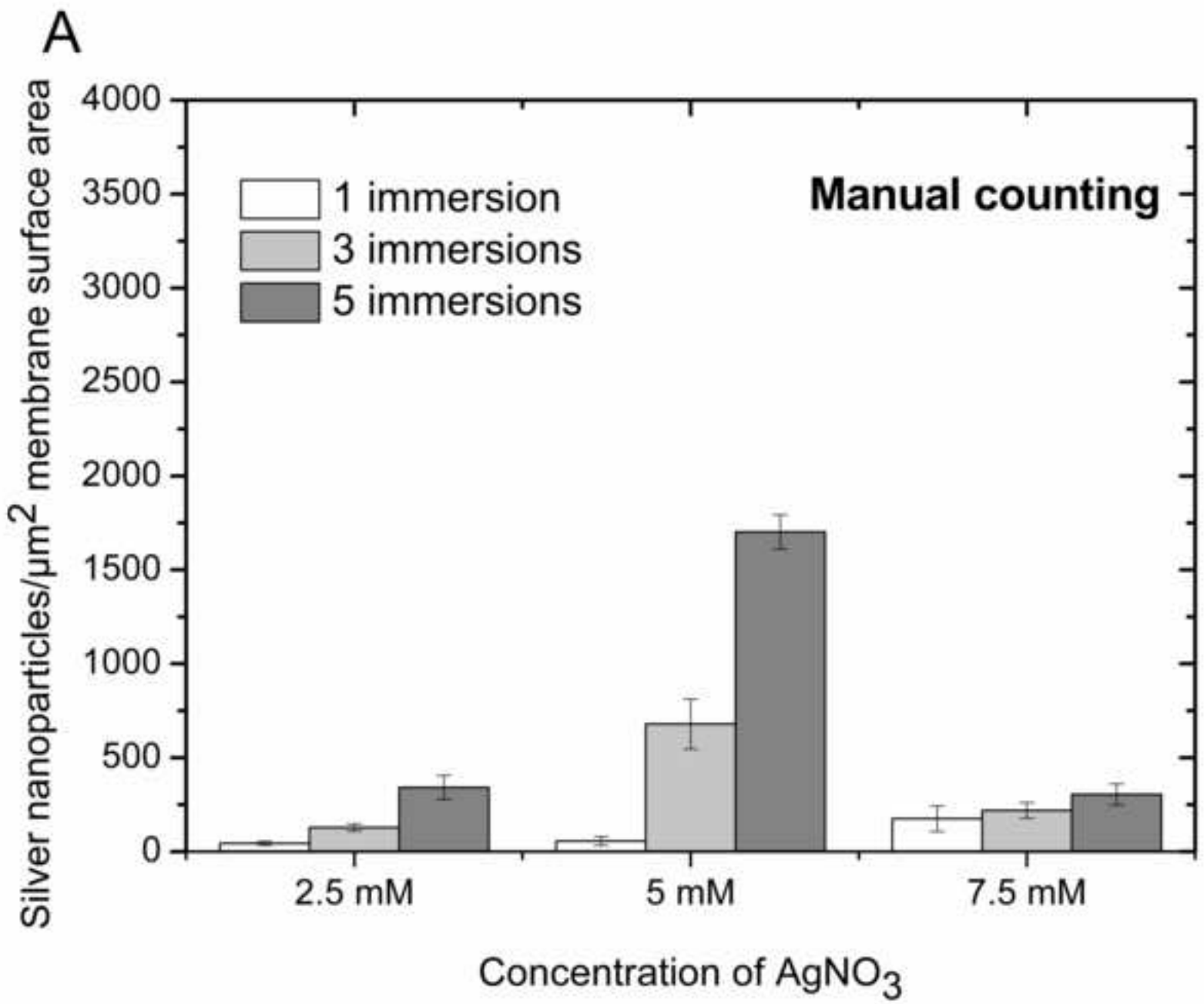

Figure 3B

Click here to download high resolution image

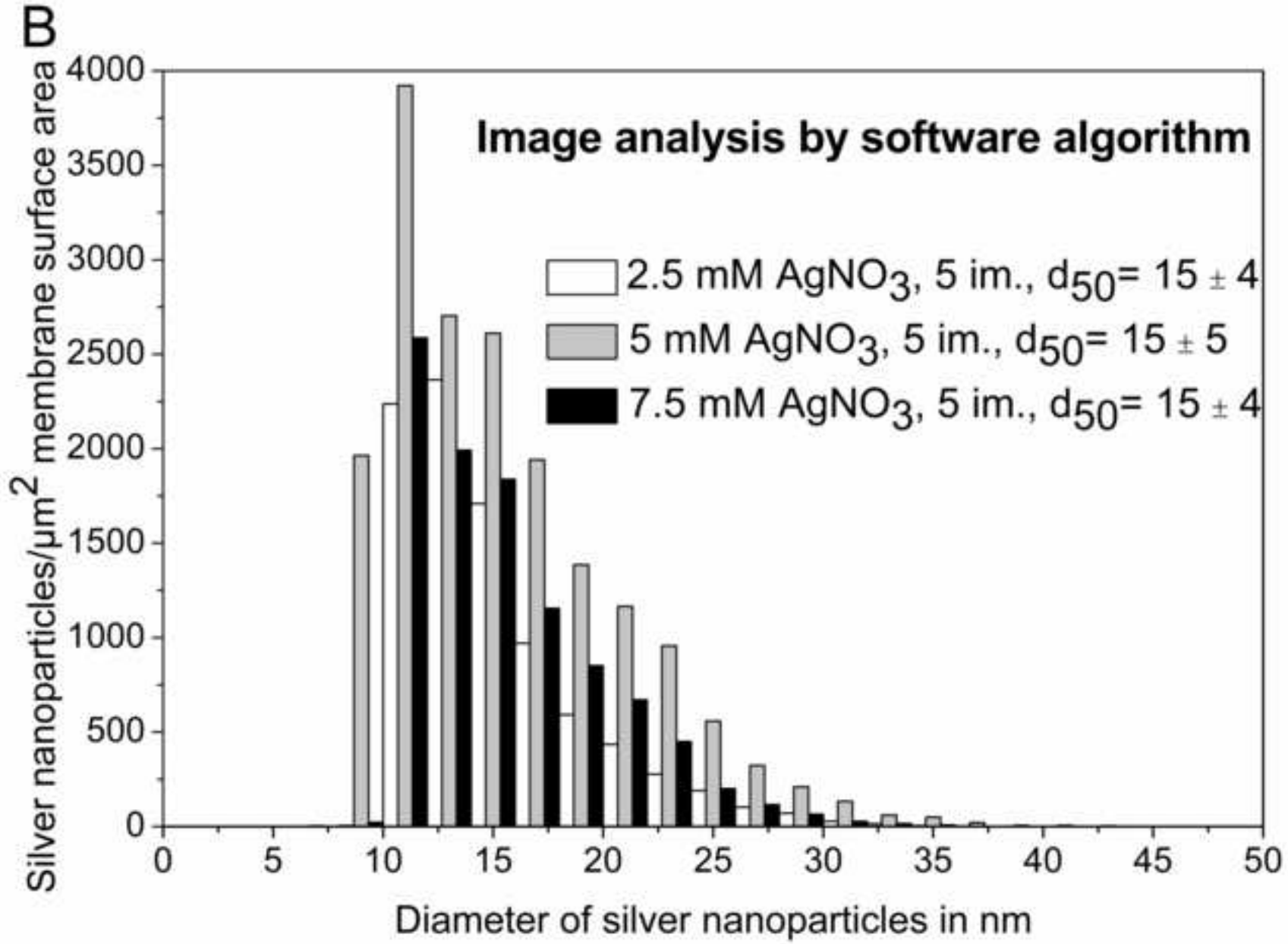

Figure 4A

Click here to download high resolution image

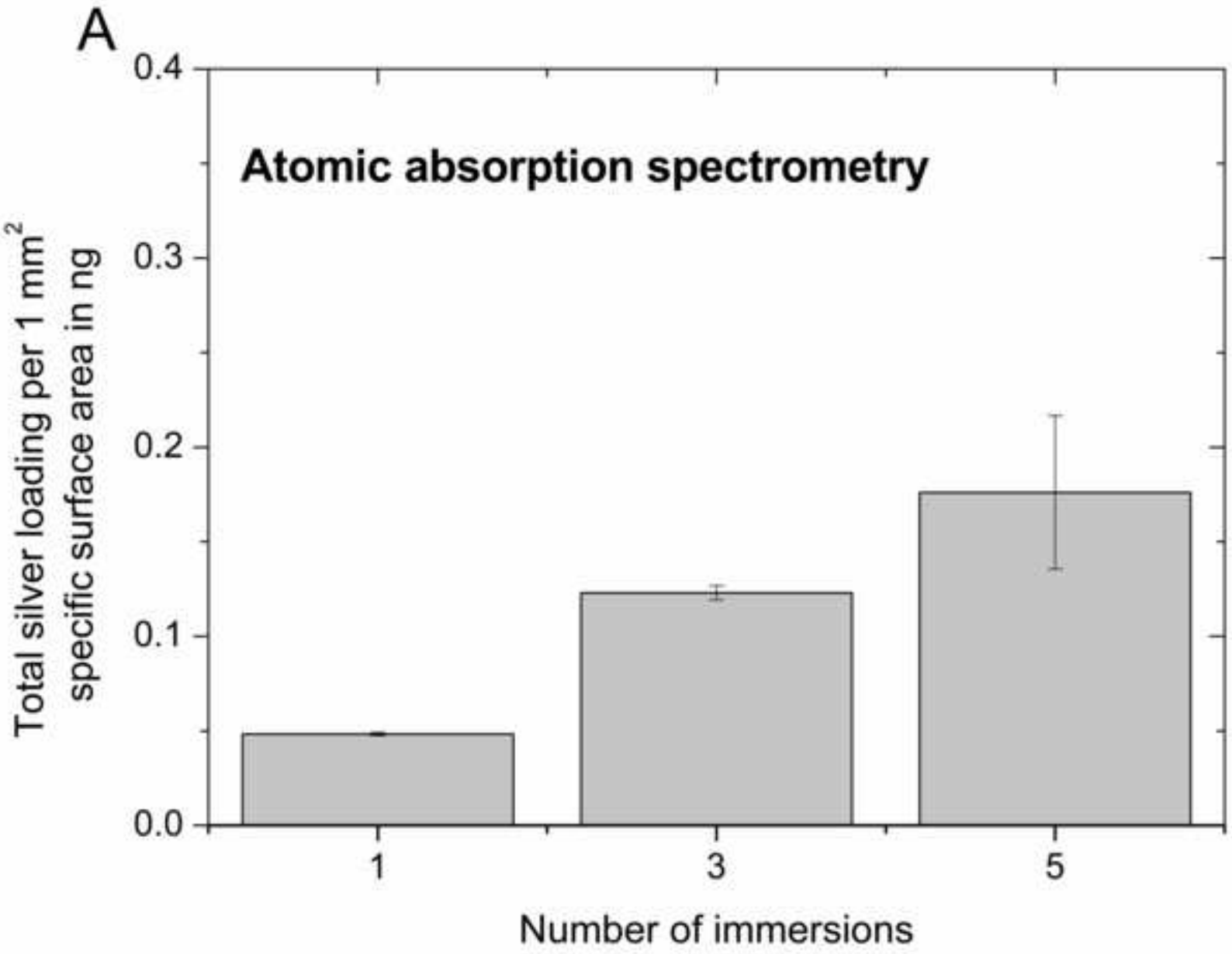

Figure 4B C
Click here to download high resolution image

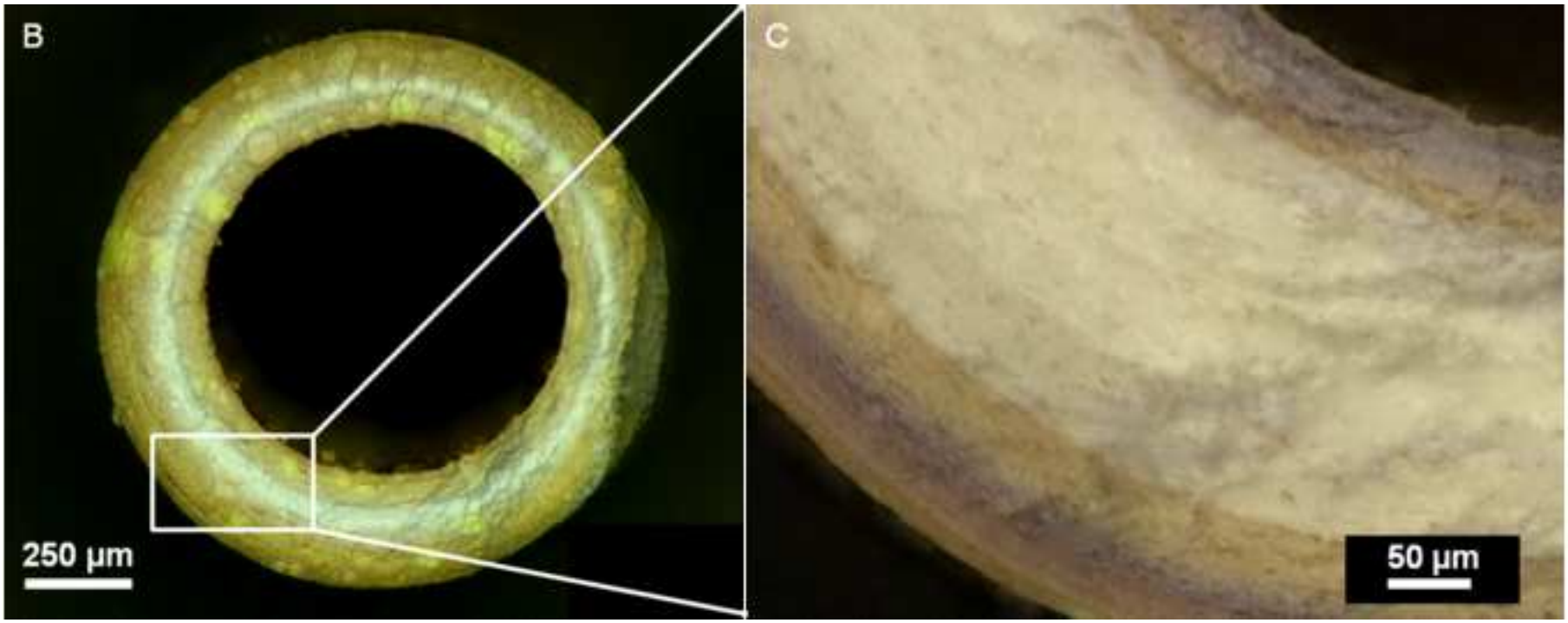

Figure 5

Click here to download high resolution image

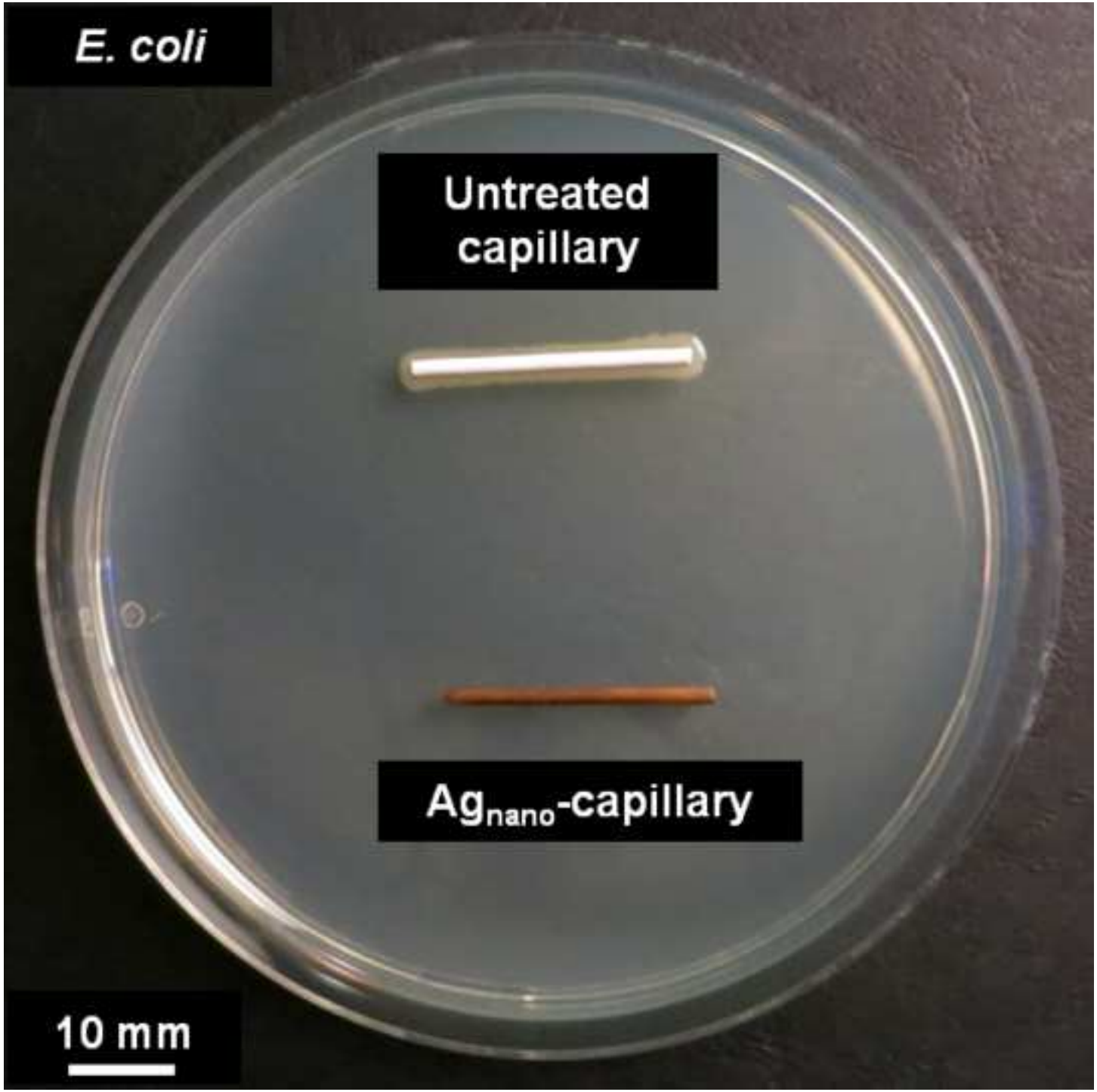

Figure 6A

Click here to download high resolution image

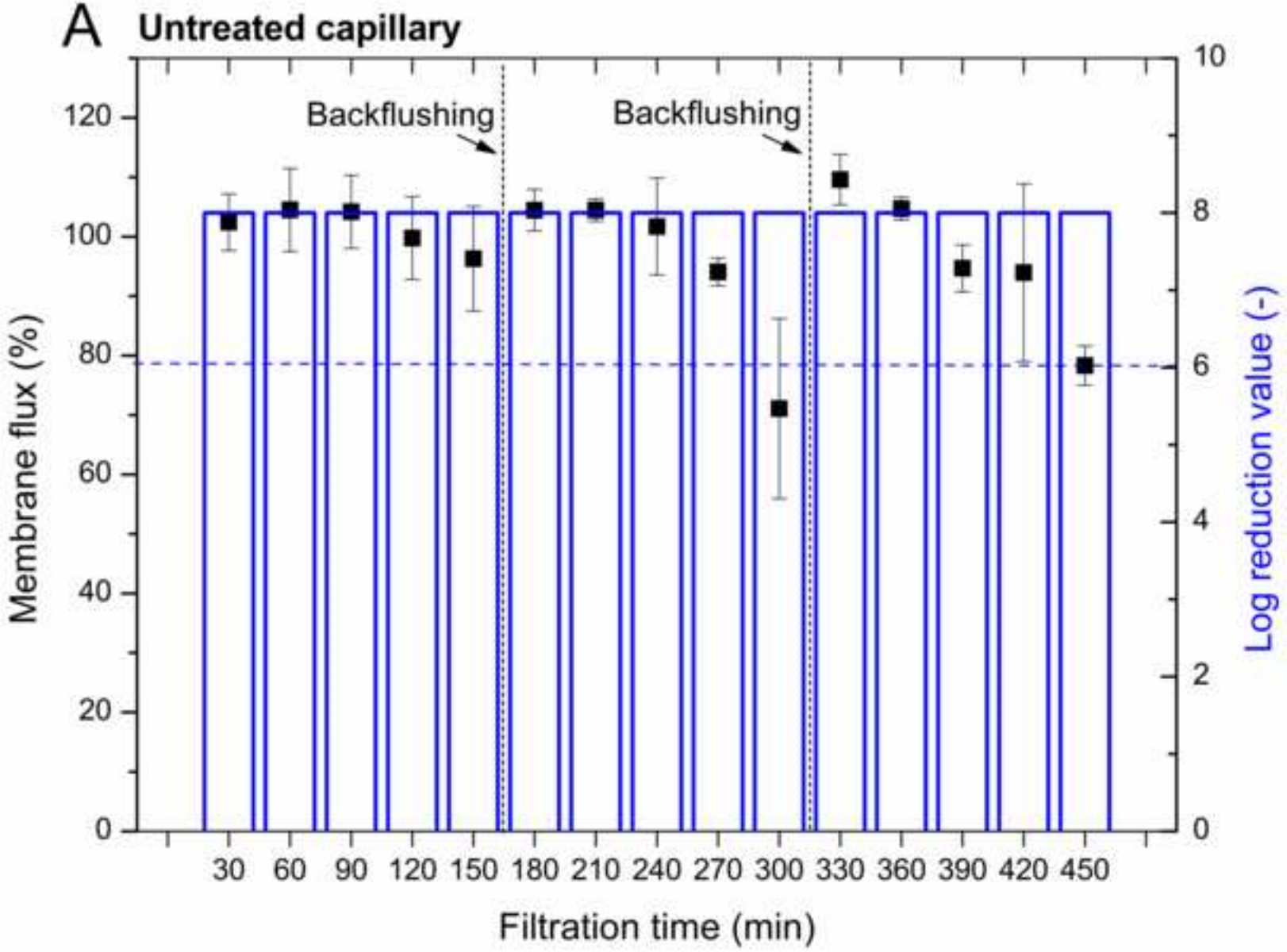

Figure 6B

Click here to download high resolution image

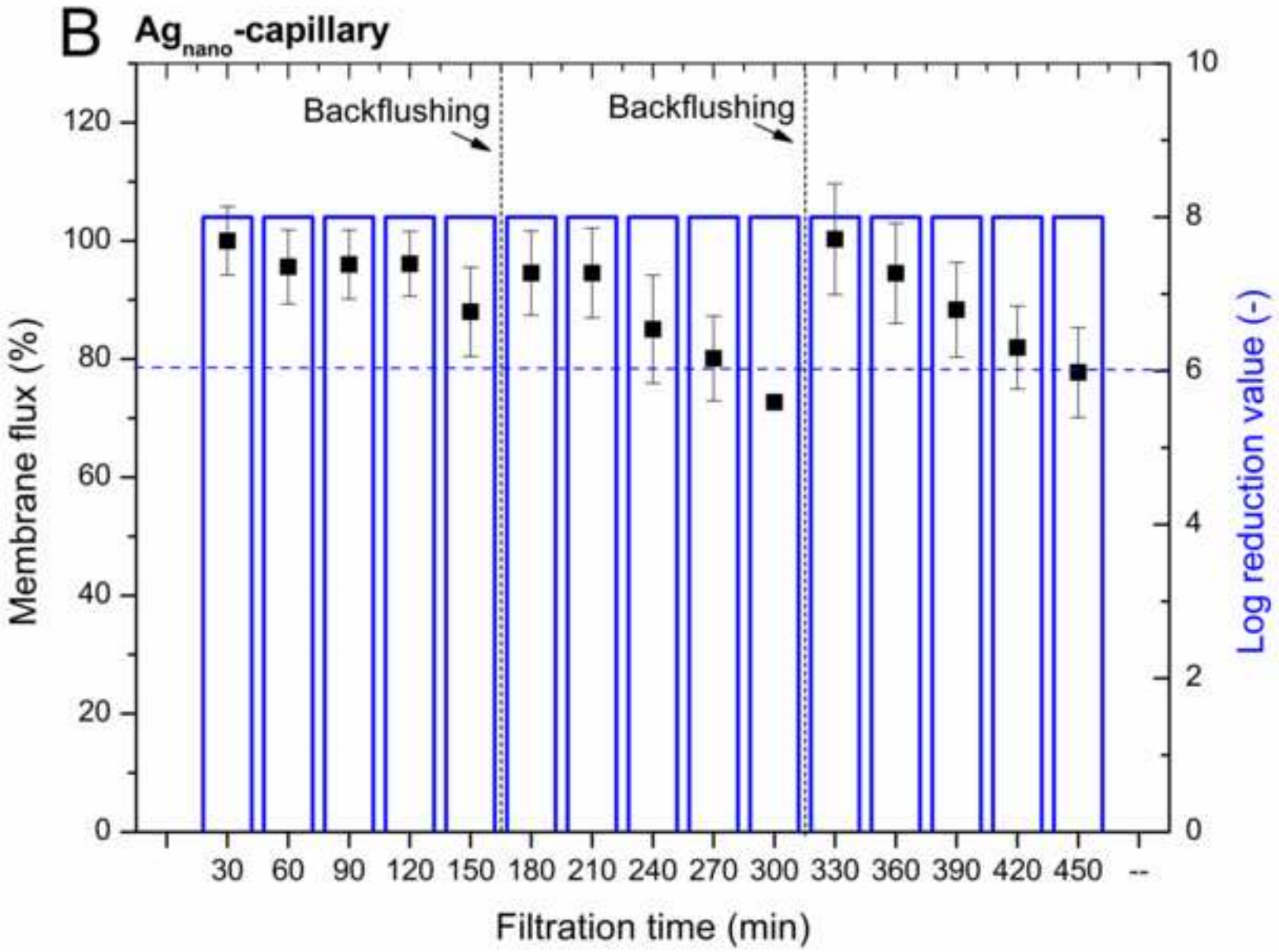

Figure 6C

Click here to download high resolution image

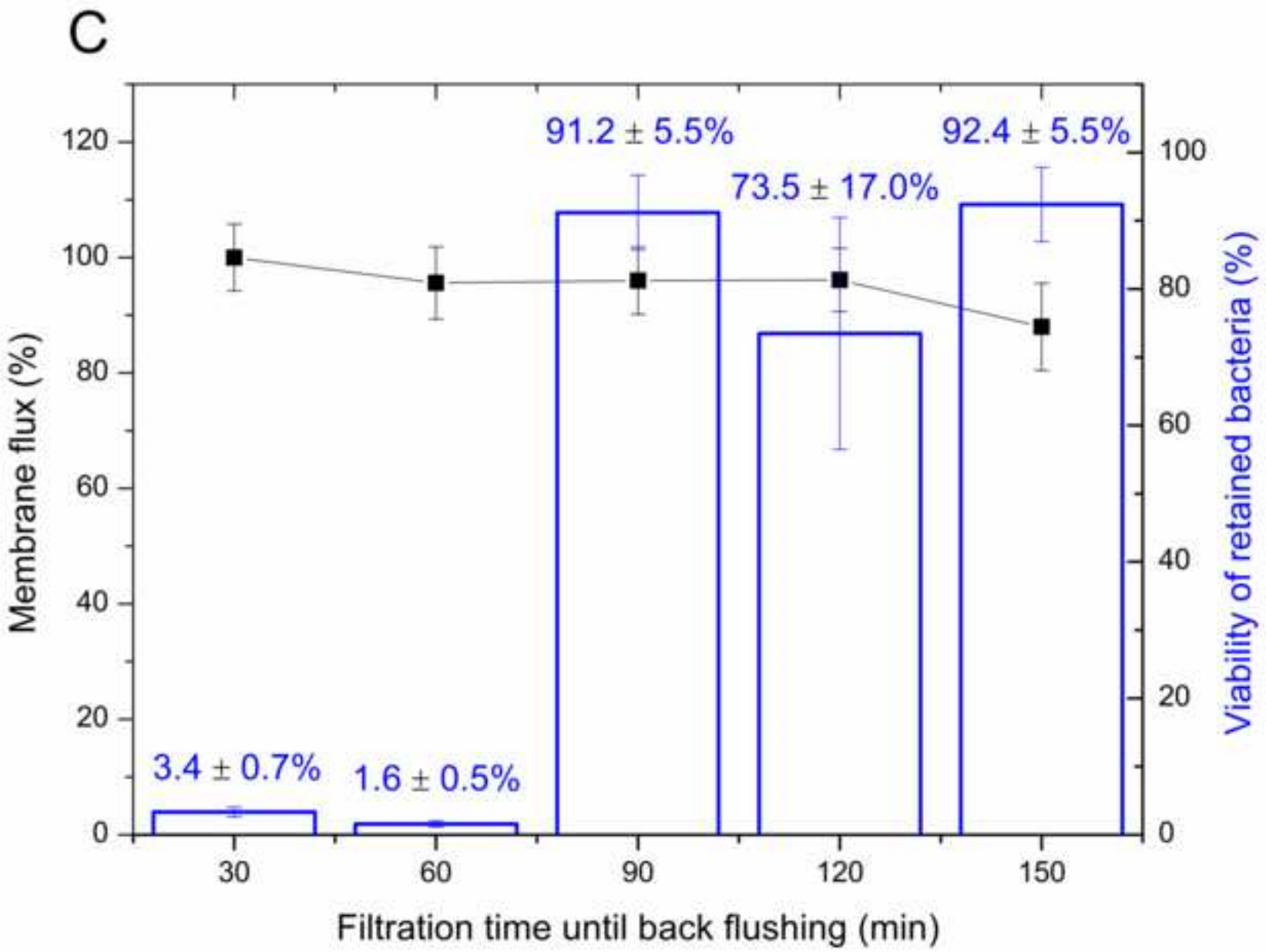

Figure 6D

Click here to download high resolution image

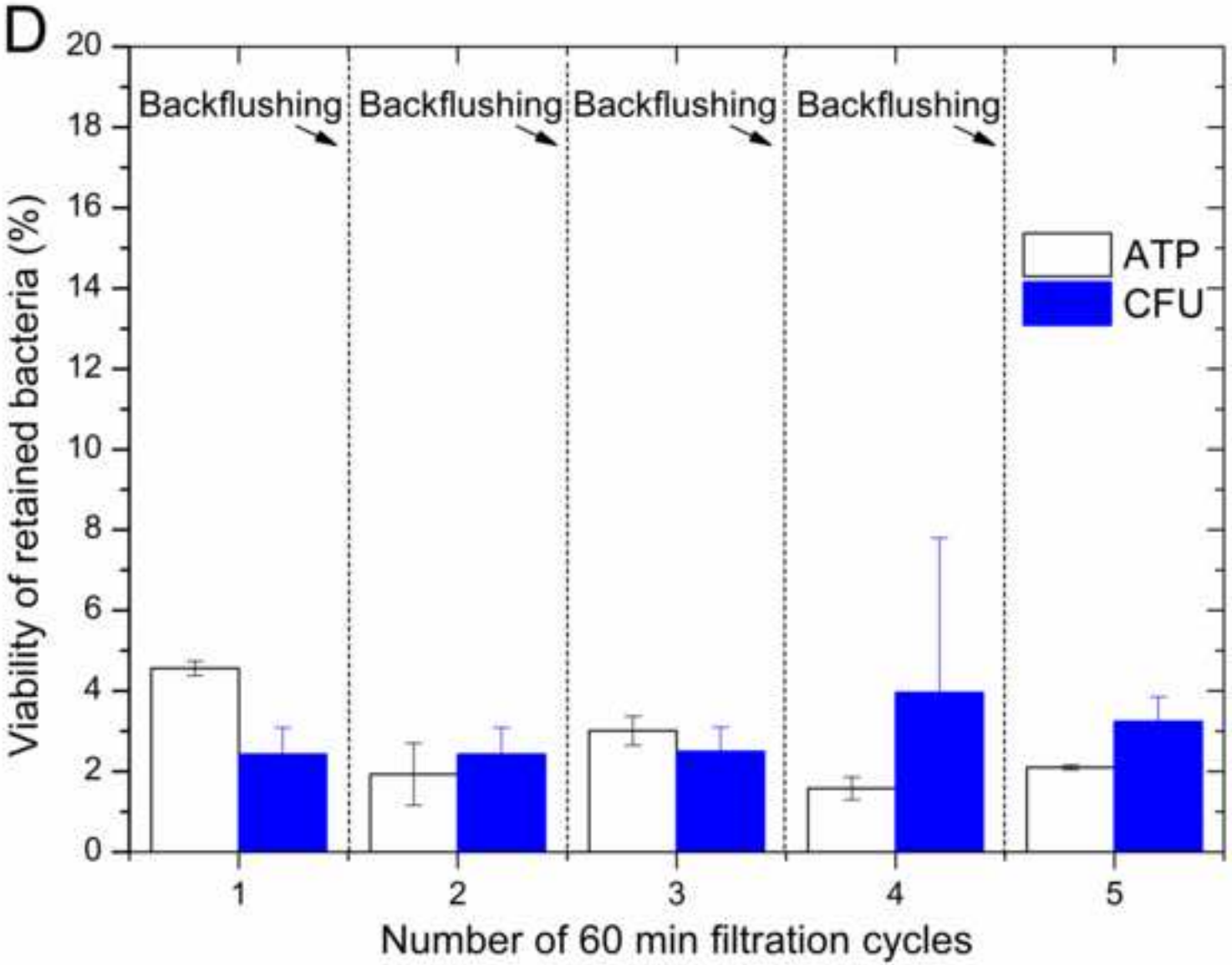

Figure 7

Click here to download high resolution image

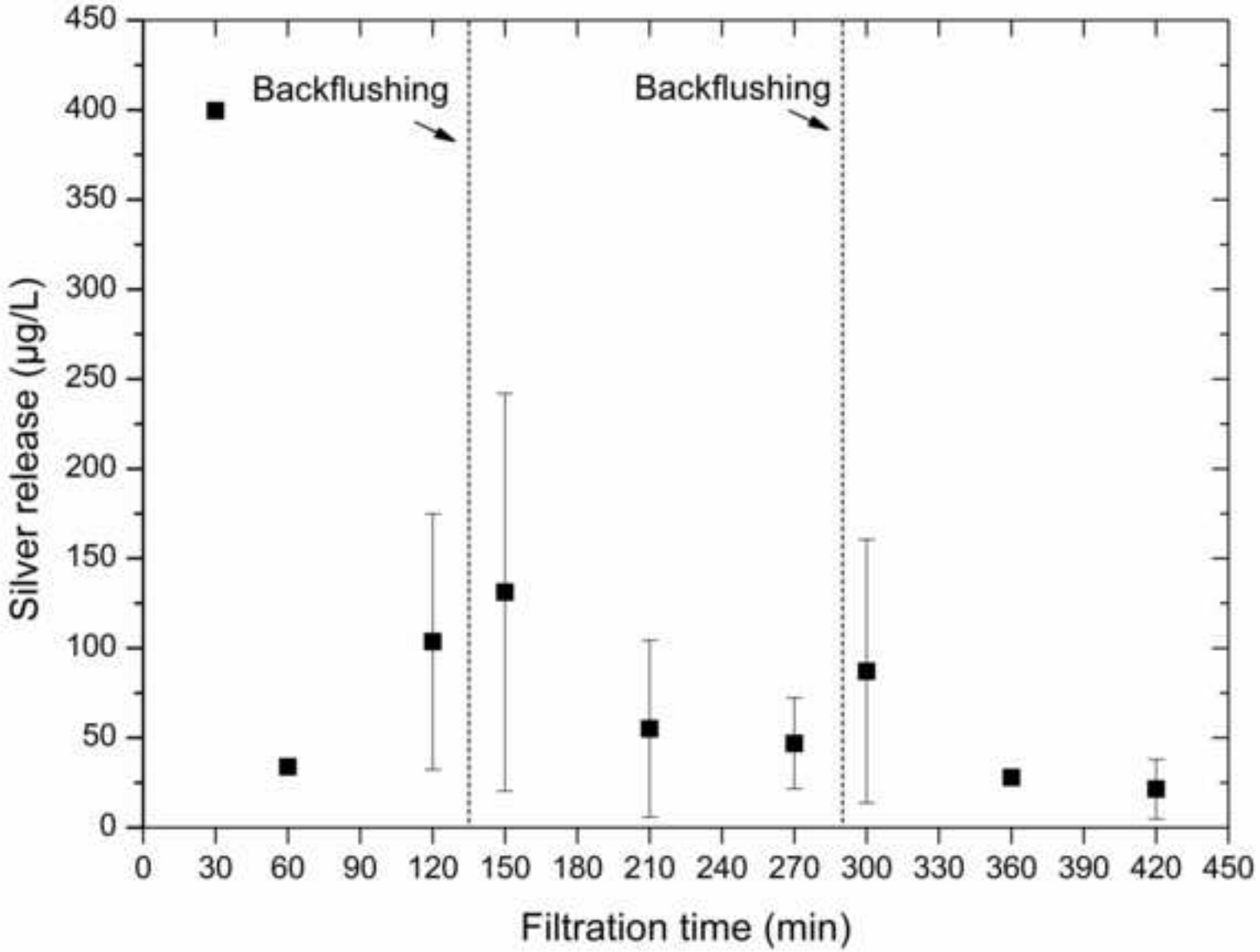

Table 1

Tab. 1: Accessible silver surface area and total amount of immobilized silver on 1 mm^2 geometric surface area of Ag_{nano}-capillaries

Conditions for the immobilization of silver nanoparticles	Accessible silver surface area in mm^2*	Total amount of silver in ng**
2.5 mM $AgNO_3$, 5 immersions	0.269 ± 0.076	8.23 ± 2.51
5 mM $AgNO_3$, 5 immersions	0.594 ± 0.129	20.00 ± 5.08
7.5 mM $AgNO_3$, 5 immersions	0.314 ± 0.101	9.95 ± 3.90

***The accessible silver surface area was calculated based on software-calculated pixel areas and on the assumption that all Ag_{nano} were spherical.**

**** The total amount of immobilized Ag_{nano} was calculated considering the density of silver (10.49 g/cm^3).**

Supplementary Fig. S1

Click here to download Supplementary Data: Wehling_Fig. S1.tif

Supplementary Fig. S2_A

Click here to download Supplementary Data: Wehling_Fig. S2_A.tif

Supplementary Fig. S2_B

Click here to download Supplementary Data: Wehling_Fig. S2_B.tif

Supplementary Table S1

Click here to download Supplementary Data: Wehling_Table S1.doc

Supplementary Table S2

Click here to download Supplementary Data: Wehling_Table S2.doc